From Medical Biochemistry and Biophysics
Karolinska Institutet, Stockholm, Sweden

NUCLEIC ACID TOOLS FOR DETECTION AND CHARACTERIZATION OF BIOLOGICAL SYSTEMS

Ioanna Smyrlaki

Karolinska Institutet

Stockholm 2022

All previously published papers were reproduced with permission from the publisher.
Published by Karolinska Institutet.
Printed by Universitetsservice US-AB, 2022
© Ioanna Smyrlaki, 2022
ISBN 978-91-8016-758-1

Nucleic acid tools for detection and characterization of biological systems

THESIS FOR DOCTORAL DEGREE (Ph.D.)

By

Ioanna Smyrlaki

The thesis will be defended in public at Samuelssonsalen, Tomtebodavägen 6, 171 65 Solna, on the 28th of October 2022, 9:30

Principal Supervisor:
Professor Björn Högberg
Karolinska Institutet
Department of Medical Biochemistry and Biophysics
Division of Biomaterials

Co-supervisor(s):
Ana Teixeira, Principal researcher
Karolinska Institutet
Department of Medical Biochemistry and Biophysics
Division of Biomaterials

Opponent:
Professor William Shih
Harvard Medical School
Department of Biological Chemistry and Molecular Pharmacology

Examination Board:
Professor Urban Lendahl
Karolinska Institutet
Department of Cell and Molecular Biology

Professor Sebastian Deindl
Uppsala University
Department of Cell and Molecular Biology

Professor Per Uhlén
Karolinska Institutet
Department of Medical Biochemistry and Biophysics
Division of Molecular Neurobiology

As you set out for Ithaka
hope the voyage is a long one,
full of adventure, full of discovery.
.
.
.
Keep Ithaka always in your mind.
Arriving there is what you are destined for.
But do not hurry the journey at all.
Better if it lasts for years,
so you are old by the time you reach the island,
Wealthy with all you have gained on the way,
not expecting Ithaka to make you rich.
Ithaka gave you the marvelous journey.
Without her, you would not have set out.
She has nothing left to give you now.
And if you find her poor, Ithaka won't have fooled you.
Wise as you will have become, so full of experience,
you will have understood by then what these Ithakas mean.

C.P. Cavafis

POPULAR SCIENCE SUMMARY OF THE THESIS

Origami technique- can it reveal the cell´s secrets?

In Japanese culture origami is the technique of folding paper in specific shapes. In this thesis we used DNA as a folding material, in order to create different shapes at the nanoscale. By combining this technique with chemical technology we are able to attach molecules on nanostructures, with result to create well defined molecular patterns.

In one of our studies, we positioned pairs of antigens (target molecules for the immune system) on the surface of a DNA origami nanostructure, to study their interaction with antibodies. Antibodies have a characteristic Y shape with two arms, which are able either to move close to each other or to stretch out into a T shape, similar to person's hands when they are doing jumping jacks. Our data showed that when the antigen distance was between 3-17 nanometers, then both arms were bound to them, but when the distance was longer than 17 nanometers the antibodies could not bind with both arms. Furthermore, we found that antibodies were able to bind the strongest to their antigens that were separated by 16 nanometers. In the future, the DNA origami technique could be used for creating patterns of antibodies, with either Y or T shapes, and explore how each shape affects functions of immune cells.

Cells communicate with other cells through protein-protein interactions on their surfaces. During this process, a different sort of touch delivers a different message to the inside of the cell. It has been shown that this message differs when the proteins form patterns of specific densities and at specific distances. In our study we created patterns of Jag1 proteins on a DNA origami, and found that when more proteins were placed on a single DNA origami then this message was delivered with greater success to the inside on the cell. This happens because when more proteins are close together, they help each other to attach on to the cell surface.

The work presented in this thesis shows that the DNA origami technique can be used to create patterns of molecules, in order to explore different cell functions that are currently unknown to us.

ABSTRACT

Nucleic acids, DNA and RNA, are naturally occurring biopolymers synthetized by cells to store and propagate genetic information. They can be found in eukaryotic cells, bacteria, archaea and viruses and, thanks to the development of synthetic chemistry techniques, they can be synthetized with relative ease on demand in the laboratory. DNA and RNA can form very distinct structures through Watson-Crick base pairing, where nucleobases form hydrogen bonds between the two antiparallel strands of a double helix. The programmability of base pairs can also be used to create pre-defined structures using nucleic acids as building material. One of the implementations of this, the DNA origami technique is using a long ssDNA oligo (scaffold) and hundreds of shorter oligonucleotides (staples) to bridge different regions of the scaffold together and form well defined shapes. DNA nanostructures generated this way can be used, among other things, as carriers of functional molecules to create patterns.

In paper I. we present a method to study the spatial tolerance of antibodies by using DNA origami structures to present nanoscale antigen patterns. The DNA nanopatterns were immobilized on a surface plasmon resonance set up and the binding kinetics of different antibodies were measured. We found that the IgG subclasses and isotypes studied, were able to bind bivalently to two antigens separated by distances between 3 to 17 nm, with a distinct preference showed for the 16nm distance. Different spatial tolerance profiles were observed for a monomeric IgM, and IgG antibodies with lower affinities to antigens.

In paper II. we use a DNA origami nanostructure to create different patterns of Jag1 ligand for studying the activation mechanism of the Notch signaling pathway. By treating induced pluripotent stem (iPs) cells with various Jag1 nanopatterns we found that bigger clusters of Jag1, induced more activation of the Notch receptors. This effect was further elucidated to occur because of prolonged binding of the ligand-receptor complex, leading to activation of Notch receptors in the absence of intercellular or external forces.

In paper III. we introduce a new method to synthesize DNA origami directly on magnetic beads. Our method, tested for a variety of different DNA origami structures, can achieve up to 90% yield compared to a standard folding protocol. Additionally, the same solid support can be used to functionalize the DNA origami in a one-pot-reaction and purify them from the excess of the molecules.

In paper IV. we present a protocol for detecting viral RNA in patient samples with Covid19 by circumventing the RNA extraction step, which was a bottleneck in the detection process at the beginning of the pandemic. Samples were inactivated by heat and the RT-PCR was performed directly (hid-RT-PCR). By comparing our results with the standard diagnostic method on 597 clinical samples we concluded that hid-RT-PCR is a reliable simplified and cost-efficient method that could increase diagnostic availability and subsequent decrease in spread of the virus.

LIST OF SCIENTIFIC PAPERS

I. Alan Shaw, Ian T. Hoffecker, **Ioanna Smyrlaki**, Joao Rosa, Algirdas Grevys, Diane Bratlie, Inger Sandlie, Terje Einar Michaelsen, Jan Terje Andersen & Björn Högberg. Binding to nanopatterned antigens is dominated by the spatial tolerance of antibodies. Nature Nanotech 14, 184–190 (2019)

II. **Ioanna Smyrlaki**, Ferenc Fördös, Iris Rocamonde Lago, Yang Wang, Antonio Lentini, Bjorn Reinius, Ana Teixeira and Björn Högberg. Clustering effect of Jag1 ligand on Notch signaling pathway. Manuscript

III. **Ioanna Smyrlaki**, Alan Shaw, Yunshi Yang and Björn Högberg. Solid Phase Synthesis of DNA Nanostructures in Heavy Liquid. Manuscript

IV. **Ioanna Smyrlaki***, Martin Ekman*, Antonio Lentini, Nuno Rufino de Sousa, Natali Papanicolaou, Martin Vondracek, Johan Aarum, Hamzah Safari, Shaman Muradrasoli, Antonio Gigliotti Rothfuchs, Jan Albert, Björn Högberg & Björn Reinius. Massive and rapid COVID-19 testing is feasible by extraction-free SARS-CoV-2 RT-PCR. Nature Communications 11, 4812 (2020)

*Equal Contribution

Scientific papers not included in the thesis

I. Ian T. Hoffecker, Alan Shaw, Viktoria Sorokina, **Ioanna Smyrlaki** & Björn Högberg. Stochastic modeling of antibody binding predicts programmable migration on antigen patterns. Nature Computational Science **2**, 179–192 (2022)

CONTENTS

LIST OF ABBREVIATIONS

18HB	18-helix bundle
A	Adenine
BCR	B-cell antigen receptors BCR
C	Cytosine
CRD	Cysteine rich domain
Dig	Digoxigenin
DNA	Deoxyribonucleic acid
Dox	Doxorubicin
DR5	Death receptor 5
E	Envelope
Fab	Antigen binding fragments
FcγR	Fcγ receptors
G	Guanine
HB	Hollow Brick
hid-RT-PCR	Hear inactivated direct RT-PCR
IgG	Immunoglobulin G
iPs	Induced pluripotent stem
JNPs	Jag1 nanopatterns
K10	Oligolysine
LNR	Lin12-Notch repeats
N1	Nucleocapsid
NICD	Notch intracellular domain
Nip	4-hydroxy-3-iodo-5-nitrophenylacetate
Np	4-hydroxy-3-nitrophenyl
NRR	Negative regulatory region
pen/strep	Penicillin and streptomycin
PLA	Proximity ligation assay
PSPR	Patterned surface plasmon resonance
R	Rectangle
RdRP	RNA-dependent RNA polymerase
RNA	Ribonucleic acid
RT	Room temperature
RU	Response units
SPR	Surface Plasmon resonance

SPT	Sodium polytungstate
T	Thymine
TAD	Transcription activation domain
TEM	Transmission Electron Microscopy
U	Uracil

1 LITERATURE REVIEW

1.1 NUCLEIC ACIDS

Nucleic acids are naturally synthesized biopolymers, which are produced by cells to store and convey the genetic information in living organisms[1]. As a polymer it is composed of repetitive monomeric subunits, the nucleotides: guanine (G), cytosine (C), adenine (A), thymine (T) or uracil (U). The chemical structure of each nucleotide contains a five carbon sugar molecule, a phosphate group and a nucleobase. When the sugar is a deoxyribose, the polymer is called deoxyribonucleic acid (DNA) (Figure 1a) while when the sugar is a ribose, the polymer is called ribonucleic acid (RNA) (Figure 1f). Nucleic acids form long chains with directionality through connecting the 3' carbon atom of one nucleotide, with a phosphodiester bond, to the 5' carbon atom of the next nucleotide.

DNA forms mainly a right handed double helical structure, when two long polynucleotide chains, with complementary sequences, bind together with hydrogen bonds (Figure 1d). The nucleobases of one strand bind with Watson-Crick base pairing with the nucleobases of the antiparallel strand (A-T and G-C) (Figure 1b and 1c). The most commonly found form of DNA in cells is the B-DNA, which has a dimeter of 20 Å, length of 3.4 Å per base pair and takes about 10.5 bases to make one full turn. Alternative less common forms of DNA are A-DNA, which is shorter and wider than B-DNA, and Z-DNA, which is a left handed and more elongated version of DNA. In RNA, chains of nucleotides form mainly a right handed single strand helix (Figure 1e). Secondary structures of RNA can form when a single strand RNA base pairs between its complementary regions to create double stranded regions (A-U and G-C) (Figure 1g and 1h).

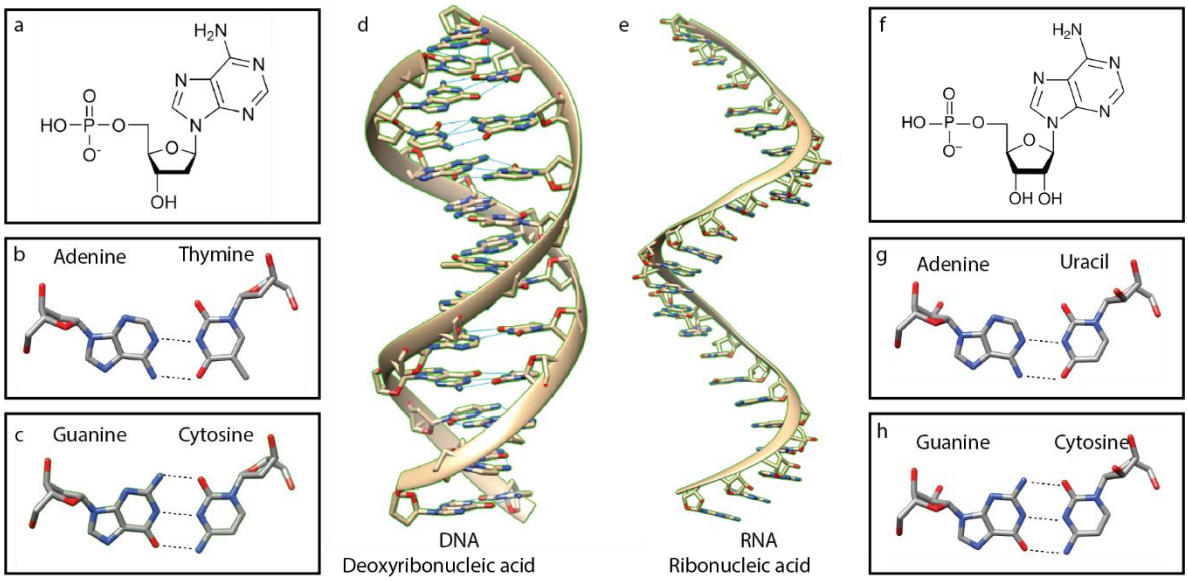

Figure 1: DNA and RNA structures. a) Structure of a deoxyribonucleotide b) structures of adenine and thymidine forming two hydrogen bonds c) structures of guanine and cytosine forming three hydrogen bonds d) structure of a double strand B-DNA (PDB ID: 7RQT) e) structure of a single strand RNA (PDB ID: 7VFT) f) Structure of a ribonucleotide g) structures of adenine and uracil forming two hydrogen bonds c) structures of guanine and cytosine forming three hydrogen bonds

The major function of nucleic acids is to store and transfer genetic information in living organisms. This information can be located in eukaryotic cells, in bacteria, archaea and viruses. Some viruses carry their genetic material in different forms such as double stranded DNA[2] , single stranded RNA[3], double stranded RNA[4] or single strand DNA[5].

The entire DNA information that is present in a cell is called genome. The long DNA strands carrying the genetic information, are packed together with histones to form the nucleosome units, which further fold in packed arrays to form the chromosomes[6]. A specific region of chromosome that carries a DNA sequence which can produce a functional RNA molecule is called gene. According to the central dogma of molecular biology[7], describing the flow of genetic information in living systems, a DNA region gets unwrapped, transcribed into an RNA molecule, and then can be translated to a protein at the ribosome. DNA can also be transcribed to RNA that doesn't give rise to proteins and those are called non coding RNAs[8].

1.1.1 DNA nanotechnology

DNA, due to its appealing characteristics, can also be used as a construction material. DNA nanotechnology as a field is using rationally design nanoscale objects made of synthetic DNA, for technological and biological applications. The idea of using DNA as a building material was conceived in 1980s, when a crystallographer was looking for new tools to control molecular orientation of proteins in crystallographic studies[9]. This was based on the principle that four DNA strands with complementarity regions can form Holliday Junctions, and by assembling multiple Holliday Junction motifs using complementary sticky ends, a rigid tile structure can be created (Figure 2). The first experimental realization of this, a DNA cube like structure made of branched DNA molecules with complimentary sticky end overhangs, was published 10 years later[10]. The next step was to create more complex periodic two dimensional structures using DNA double crossovers[11] followed by the introduction of algorithmic self-assembly to create a Sierpinski triangle pattern by using DNA computing. Three decades after introducing the idea of using DNA as a building block material, Nadrian Seeman published the first crystal structure of DNA tensegrity triangle at 4 Å resolution[12].

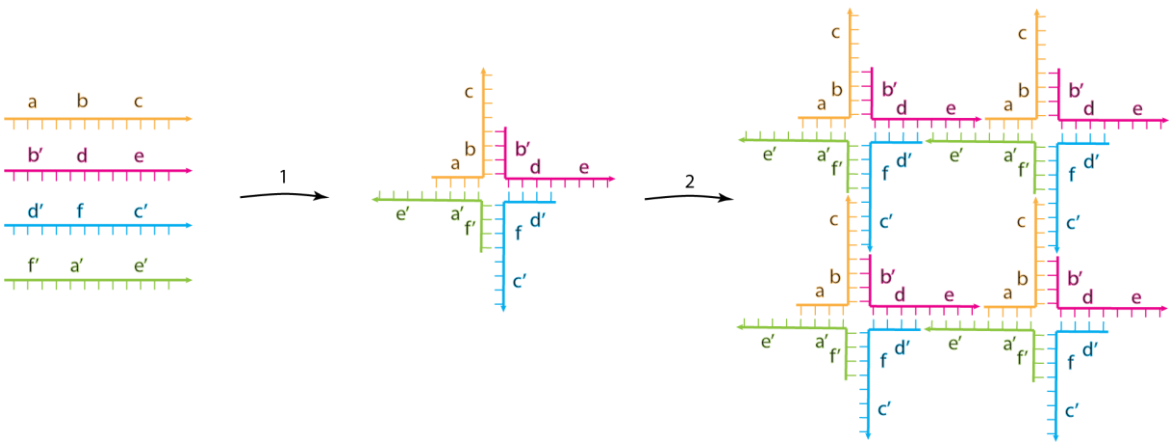

Figure 2: Holliday junction and assembly of that. Four DNA oligos with complimentary regions (a-a', b-b', c-c', d-d', e-e') can form a branched nucleic acid structure that contains four double stranded arms joined together (1). Assembly of a DNA lattice structure by mixing DNA strands with complementary regions (2).

1.1.2 DNA origami

The tile based DNA nanostructures fold by using many short oligonucleotides which very often results in low folding yield and purity. In order to eliminate these issues, the idea of mixing a long single stranded DNA with shorter synthetic oligonucleotides to form an octahedron was introduced[13]. In 2006 the scaffolded DNA origami technique was developed, where a long 7-kilobase single stranded scaffold, derived from M13mp18 phage genome, was mixed together with 200 short oligonucleotides (staples) to form many 2D shapes[14] (Figure 3).

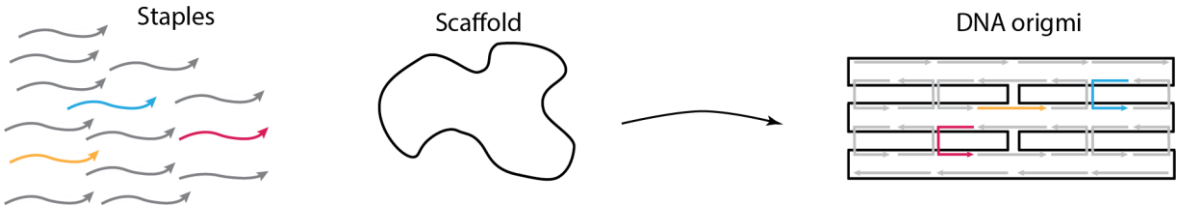

Figure 3. Schematic representation of scaffolded DNA origami technique. A long ssDNA scaffold is mixed with hundreds of short oligonucleotides, called staples, to form a DNA origami.

The same principle was later used to form three dimensional complex structures with a diameter up to 100nm, as well as homomultimeric linear polymers and heterodimeric wireframe icosahedra[15]. A significant step to the development and propagation of the DNA origami field was the release of an open-source software, caDNAno, which allows the design of DNA origami nanostructures built from helices constrained in honeycomb[16] or square lattice[17]. By inserting or deleteing bases at specific positions of the DNA helices, twisted or curved DNA origami structures can be formed which can further lead to complex circular structures, spherical balls or other complicated shapes[18,19]. One drawback of DNA origami nanostructures with packed helices is that they require the addition of Magnesium (Mg^{2+}) or Sodium (Na^{+}) during the folding process, which results in unstable structures when we apply them in biological systems. To surpass this limitation, a technique to design polygonal wireframe DNA origami was developed, resulting in more stable DNA origami structures under physiological conditions[20,21]. To produce these wireframe structures, we create polygonal meshes of the desired structures and then the software will generate the appropriate scaffold routeing and staples to fold it[20]. Although, wireframe DNA origami nanostructures have higher stability at low salt conditions, they tend to be more flexible compared to lattice based DNA origami. This flexibility can be minimized with careful considerations, regarding edge length, number of nicked edges and monovalent salt concentrations[22].

1.1.3 Functionalization of DNA origami

DNA origami technique can be used for positioning functionalized molecules at predefined and well-designed positions. The hundreds of staples, that hold together a long scaffold sequence, occupy a known position in the 3D DNA nanostructure. Staples can easily be replaced during the folding process either with functionalized staples or with longer staples that can protrude outside the structure (Figure 4). The functionalized staples can carry chemical compounds, fluorophores for microscopy applications or aptamers for biological applications. The second approach for functionalizing nanostructures, uses oligos that protrude outside the structure, and that can be used to hybridize to a complementary oligonucleotide which can carry bigger molecules like proteins.

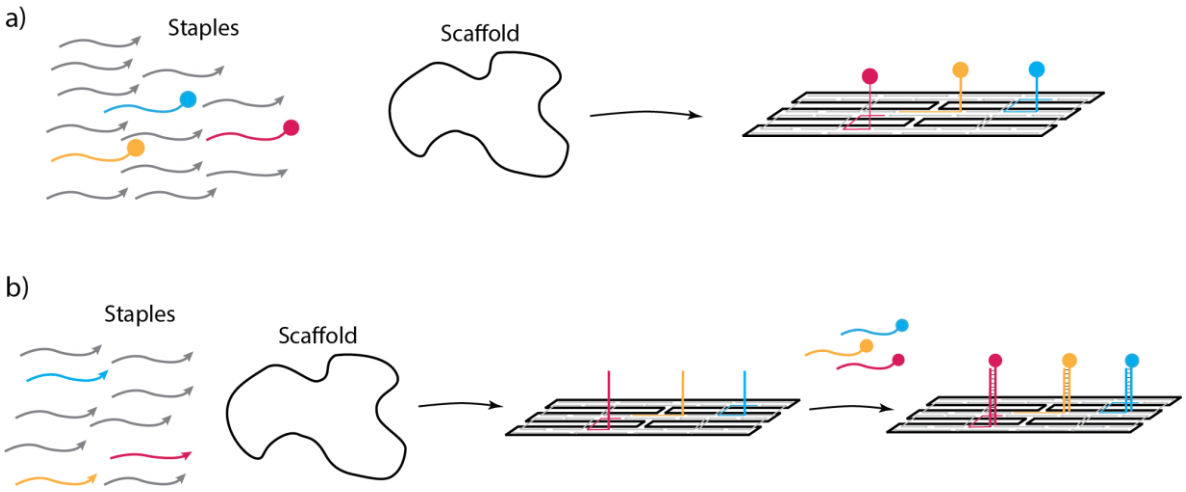

Figure 4. Functionalization of DNA origami. Functionalization of DNA can achieved a) by direct use of modified oligos during folding reaction or b) by folding the structure with oligos protruding outside the structure and then hybridize them with complementary sequences on protein-DNA conjugates

Several approaches for conjugating proteins with oligonucleotides have been developed over the past years. Some of them target specific regions of the proteins while some others bind in non-specified regions. One method that can be used to modify any available protein without special modifications, is to react the primary amines of lysine residues with NHS esters[23]. This approach results in a high conjugation yield but low specificity on the modification site. Other approaches require the expression of proteins with specific tags in a desired position. Such tags are 1) SNAP-tags[24], 2) Halo-tags[25], 3) CLIP-tags[26] and 4) SpyTag/SpyCatcher[27] system which provide high yield reactions. Although, these tags are big (>20kDa) which sometimes can be a limitation for DNA nanotechnology. Alternatively, proteins can get expressed with unnatural amino acids (UAA) to functionalize with bio-orthogonal reactions with amber-codon-suppression incorporation[28]. Production of proteins with amber suppression codon results usually in lower yield, compared to expression of native proteins. However, we can express proteins with specific amino acid sequences that will facilitate the substrate for enzymatic reactions. For example, the enzyme lipoic acid ligase (Lp1A) can recognize a 13 amino acid sequence[29] and the enzyme sortase A can ligate an oligo-glycine peptide to the LPXTG sequence[30]. Many approaches for conjugating a DNA oligo to a protein exist, and the most suitable should be chosen according to the protein availability and the downstream application.

1.1.4 Applications of DNA origami

DNA origami, due to its programmability with a precision on the nanometer scale, is used in a variety of applications in biochemistry, biophysics, synthetic biology and drug delivery. The driving force for the emergence of the DNA nanotechnology field was to use DNA as a controllable material for positioning proteins, and resolve their crystal structures[10]. In order to explore the rigidity of DNA nanostructures, the 3D structures of small DNA objects were studied by X-ray crystallography[12,31,32,33] and of big DNA origami with cryo-EM[34]. Although the DNA origami structures could not be resolved with high resolution on cryo-EM, they were able to function as supports for determining the structure of proteins[35,36]. A recent paper used DNA origami structures as a tag for specific proteins on the surface of vesicles, virus envelop and cells[37] and studied them with cryo tomography.

An additional application, is using DNA origami to construct molecular machines[38,39] that can either act as walking devices [40,41,42] or as a pair of tweezers[43]. These machines used toehold mediated strand displacement, base stacking or enzyme catalyzed reactions, in order to induce changes on the structures. Another way to control the dynamic conformational changes of DNA nano-devices, is by changing the cation concentration[44]. In this case, the DNA devices were forming open states at low Mg^{2+} and closed states at higher Mg^{2+} concentrations. Recently, a DNA molecular printer composed of three DNA origami linear actuators, was used to create a nanoscale robotic printer[45]. DNA origami because of their ability to undergo conformational changes, can apply and detect forces in biological systems. For example, a hinged DNA origami, that is able to position molecules down to the Bohr radius level[46], was used to explore the forces between nucleosomes[47].

The characteristic of DNA origami to carry molecules with high programmability, created applications in the drug delivery field, where a nanostructure can be used either to kill abnormal cells or to reduce the side effects of the drugs. In one case, the chemotherapeutic agent anthracycline doxorubicin (Dox) was loaded on two DNA nanostructures with different degrees of twist, where different release rates of the drug were observed on breast cancer cells[48]. The same drug, anthracycline, when was combined with DNA origami structures, circumvented Drug Resistance in various cells lines[49,50] and in vivo[51]. In another example, DNA origami structures were used as carriers of drugs that carry a logic gate for opening and releasing the drug after sensing the environment in vitro[52] and in vivo[53]. To further expand the studies for in vivo drug delivery of DNA origami, protection of the DNA origami from nuclease mediated degradation is necessary. To improve the in vivo bio distribution of DNA origami, coating with PEGylated lipid bilayers[54] or oligolysine-PEG solution[55] is important.

Several applications use DNA origami in order to position proteins and control their functions. For example, cells are known to compartmentalize enzymes, in order to increase the efficiency of their reaction. To control the spatial arrangement of multienzyme cascades with distance specificity for each enzyme, a DNA origami was used as a scaffold[56,57,58]. DNA nanotechnology was also used in order to protect enzymes. In this case, by using a DNA nanocage, increased protection against proteases was achieved[59] and also allowed the controllable accessibility of the enzymes[60].

1.1.4.1 Spatial arrangement of receptors utilizing DNA origami

The ability of DNA origami display proteins at well-defined positions, made it an attractive tool to study signal transduction. Cells communicate with the extracellular environment to initiate cellular events by forming spatial arrangements of receptors on the membrane. Such an example is the Ephrin receptor, which regulates cell migration and proliferation by recognizing their ligands on adjacent cells[61]. To study the effect of spatial arrangement of ligands on receptor activation, a DNA origami nanocalliper was used to present Ephrin A5 ligands at specific distances[62]. The effect of Ephrin A5 nanocalipers was later studied with sequencing technique as well, and divergent transcriptional responses were observed[63]. In another study, DNA origami was used to study the nanoscale arrangement on EGF receptor activation with patterned DNA nanostructures decorated with their ligands, using microarrays[64]. Moreover, DNA microarrays with immobilized DNA origami were used to study the cooperativity effect of integrins with EGF receptors[65] while cluster formation of integrin receptors was recently

explored by using Multivalent DNA-Based Nanoparticles[66]. Death receptor 5 (DR5), a receptor that belongs to the tumor necrosis factor receptor superfamily, was found to require dimerization or trimerization of its transmembrane domain, suggesting that bigger interaction networks of receptors with ligands[67] are necessary to induce apoptosis. When hexagonal patterns of DR5 ligands displayed at 5nm inter-ligand distance on a DNA origami nanostructure, death receptor clustering and a resulting apoptosis was observed[68]. An additional study for FasL death receptor, showed that hexagonal FasL arrangements present on DNA origami with 10 nm inter molecular spacing, exhibit higher efficiency than soluble ligands or different pattern arrangments[69].

1.2 MOLECULAR PATTERNS IN BIOLOGICAL SYSTEMS

1.2.1 Immunology

Molecular patterns are important in both innate and adaptive immune system[70]. A key element of these systems is the interaction between antigen and antibodies. Antibodies, also known as immunoglobulins, affect the immune system through their ability to neutralize pathogens. They have a characteristic "Y" shape, which is composed of two antigen binding fragments (Fab), important for binding to an antigen, and an Fc region responsible for initiating other immune responses. B cells are part of adaptive immune system and can either secret antibodies to the blood plasma or bind them with B cell receptors expressed on their surface. In humans, 5 different types of antibodies (IgG, IgM, IgE and IgA) are expressed. The most abundant isotype IgG, can divide into four subclasses (IgG1, IgG2, IgG3 and IgG4), which differ only in the length of a region that connects the Fab arm with the Fc part (hinge region) (Figure 5). This hinge region is mainly responsible for the flexibility of the Fab arms which, as shown in electron microscopy studies, can vary its conformation between a Y and a T shape[71]. Because of this characteristic, the crystal structures of full antibodies are difficult to be determined and not many are available[72].

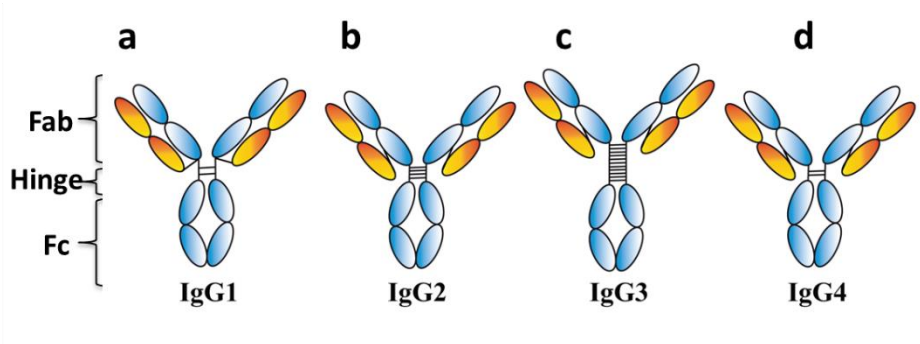

Figure 5. Schematic illustrations of the human IgG1 subclasses. a) IgG1 b) IgG2. c) IgG3. d) IgG4. Each IgG subclass is composed of two heavy chains and two light chains that are colored blue and orange, respectively. The heavy and light chains are covalently bound via disulfide bridges. An antibody can be divided onto three main parts, the constant Fc that is linked to two Fab arms via the hinge region (represented with lines). The number of disulfide bridges varies between the IgG subclasses.

Multivalent antigen arrangements are important for antibody mediated immune responses. The protein C1q initiates complement activation upon binding on hexamers of immunoglobulin G (IgG)[73]. Multivalent interactions between antigens-antibodies are also important for antibody-

dependent cell-mediated cytotoxicity and antibody-mediated antigen presentation[74,75]. Furthermore, multimers of antigens can also initiate B-cell signaling though B-cell antigen receptors (BCR)[76]. Specifically, bi- and trivalent haptens (small antigens) activated the BCR whereas monovalent haptens were ineffective[77].

1.2.1.1 Molecular patterns in immunology utilizing DNA origami

The ability of DNA origami to present any molecule at various distances and configurations, made it a great tool to study immunological responses. In an exemplary work, the immunogen eOD-GT8, an engineered outer domain of the HIV-1 glycoprotein-120, was displayed on DNA origami to study the effect on B-cell activation[78]. In another study, to explore the spatial arrangement of PD-L1 ligands on T-cell inhibition, a DNA origami flat sheet with various PD-L1 ligand configurations was utilized to regulate T-cell signaling[79]. DNA origami structures were also used for presenting CpG-motifs at 7nm distance, and high immune activation achieved by binding to Toll-like receptor 9 on macrophages[80]. Macrophages destroy pathogens through antibody-optionization mediated by Fcγ receptors (FcγR). Another study using DNA origami showed that macrophages probably sense ligand densities to make engulfment decisions[81].

1.2.2 Notch signaling pathway

Notch signaling co-ordinates cell fate decisions of neighboring cells though direct cell-cell contact. During development it co-ordinates differentiation by directing lateral inhibition, asymmetric cell divisions, tissue patterning, angiogenesis and neurogenesis. The contact area between the two cells was found to affect the signal by using micro-patterning of Notch receptors[82]. It has been shown that mutations on the receptors or its ligands structures, can lead to genetic disorders and cancer.

To better understand the mechanism of this pathway we need to take a closer look to its components. In mammals, four types of Notch receptors are expressed (Notch1-4) and two families of ligands: Serrate (Jag1 and Jag2) and Delta (DLL1, DLL3 and DLL4). Activation of this pathway relies on three proteolytic cleavage steps. During maturation at the Golgi, the Notch receptor is cleaved by furin-like convertase (S1) to form a non-covalently associated heterodimer which then translocates to the cell surface. There, upon interaction with its ligands expressed in the adjacent cell, the second cleavage occurs by ADAM metalloproteases (S2) and a subsequent intracellular cleavage by γ-secretase (S3). These events lead to the release of the Notch intracellular domain (NICD) which can translocate to the nucleus to assemble with a DNA binding protein of CSL family and the co-activator Mastermind, and act as a transcriptional activator (Figure 6).

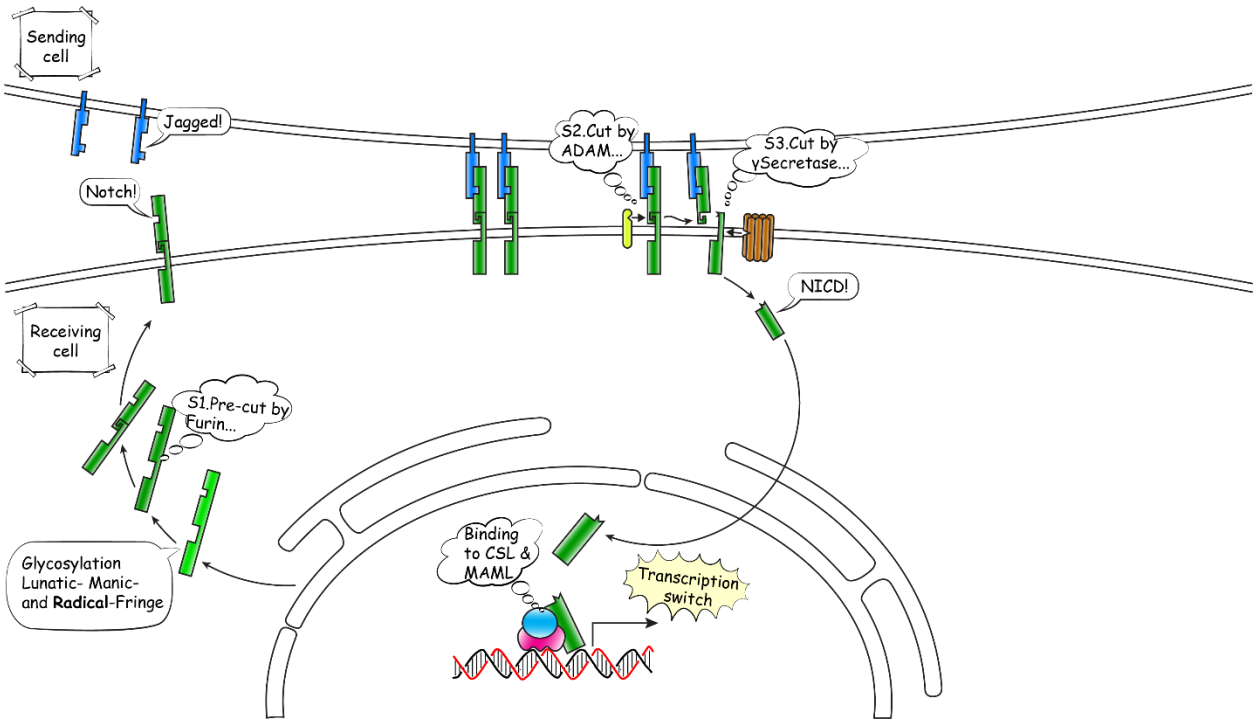

Figure 6. Schematic diagram of Notch signaling pathway. The Notch receptor maturates at the Golgi where is cleaved by furin-like convertase (S1) to form a non-covalently associated heterodimer which then translocates to the cell surface. Upon interaction with its ligands expressed in the adjacent cell, the second cleavage occurs by ADAM metalloproteases (S2) followed by an intracellular cleavage by γ-secretase (S3). The notch intracellular domain (NICD) is released and translocates to the nucleus to act as a transcription factor.

The Notch receptors are big molecules and each region has a discreet function. The extracellular part is composed of EGF repeats (29-36), which can either facilitate their interactions with ligands or bind calcium ions to determine the affinity of ligand binding, followed by three cysteine-rich Lin12-Notch repeats (LNR) and a hydrophobic heterodimerization domain which are known together as negative regulatory region (NRR). The NRR region is located next to the cell membrane and forms a loop to protect the S2 site from ADAM mediated cleavage[83]. The S3 site is located within the transmembrane segment and controls the release of the NICD. The NICD contains a RAM domain, seven ankyrin repeats which are involved in CLS interaction at the nucleus, a transcription activation domain (TAD) and a PEST region responsible for NICD degradation. Ligands of Notch are also single pass transmembrane proteins. The structure of Notch ligands contains a DSL domain at the N-terminus and EGF-like repeats (16 for Jagged family and 5-9 for Delta family) followed by cysteine rich domain (CRD) only in Jagged family ligands. The N-terminus of human Jagged-1 and DLL1 is a C2 phospholipid recognition domain that binds phospholipid bilayers in a Ca^{2+} dependent fashion[84]. Co-crystal structures of Notch1 and DDL4 revealed that DSL and C2 domains of DLL4 bind on EGF11 and EGF12 of Notch1[85] while C2 and EGF3 of Jag1 engage EGF8 and EGF12 respectively. This data concludes that different sites of Notch receptors are responsible for discrete interactions with specific ligands. The binding preference of Notch receptors to specific ligands is mediated by post translation modifications induced by fringe proteins, which can glycosylate their EGF repeats. In mammals, three types of fringe proteins are present: Lunatic, Manic and Radical. Fringe modifications at EGF8 and EGF12 enhance activation of Notch by DLL-1, Manic and Lunatic modified EGF6 and EGF36 inhibit Notch1 activation by Jagged1, while Radical enhances signaling from both Jag1 and DLL-1[86]. The

affinity differences between ligands, can explain ligand specific behaviors, for example, expression of DLL1 and DLL4 lead to opposing effects on muscle differentiation[87,88].

Many scientists have tried to elucidate the circumstances under which the NRR region unfolds to uncover the S2 cleavage site. The currently accepted model of canonical Notch pathway activation involves the endocytosis of ligand-receptor complex by the ligand expressing cell[89,90] which is controlled by the Epsin pathway[91]. This endocytosis occurs either for receptor recycling purposes or to exert a pulling force to uncover the S2 region of the receptor. By applying tension gauge tethers on ligands immobilized on surface, a force of 12pN was required for Notch activation[92]. The activation of Notch receptor by pulling forces was confirmed by magnetic beads tethered to Notch molecules on the cell surface[93]. The high affinity ligand DLL-4 activates Notch at tensions of 1pN while the low affinity Jag1 required tension above 4pN[94]. In the same study, when a range of tensile forces applied for measuring the lifetime of ligand-receptor bond, a catch bond behavior observed for both Jag1 and DLL-4. Dynamic expression of Notch target genes is known to be important during developmental processes. Recently, it was shown that cells use dynamics to discriminate signaling by DLL1 and DLL4 through Notch1 receptor[95]. Single cell imaging experiments revealed that DLL1 activates Notch1 in pulses to upregulate Notch target gene Hes1 while DLL4 in a sustained manner to subsequently upregulate Hey1 and HeyL genes.

Notch signaling pathway is important in many biological processes and mutations can result in abnormal activation and several diseases. Understanding of the activation mechanism is of great importance for the development of new approaches to target this pathway.

2 RESEARCH AIMS

The aim of the work presented in this thesis is to create research methods by using nucleic acids, for the characterization and detection of biological systems. The specific aim of each paper presented in the thesis is:

Paper I. – To develop a new method for studying the spatial tolerance of different antibodies, using the DNA origami technique for creating molecular patterns of antigens.

Paper II. – To investigate the effect of nanoscale spatial configurations of Jag1 ligands on the Notch receptor activation, using Jag1 patterned DNA origami nanostructures.

Paper III. – To create a new method for folding DNA origami directly on magnetic beads, which permits the removal of excess folding material, the functionalization of nanostructures with molecules and their subsequent purification in one pot reaction.

Paper IV. – To develop a new protocol for detecting RNA in Covid19 patient samples by circumventing steps in the standardized diagnostic procedure, that were cost and time consuming, with the goal to increase the diagnostic availability.

3 MATERIALS AND METHODS

3.1 FABRICATION OF PATTERNED DNA ORIGAMI

3.1.1 Design of DNA origami nanostructures

DNA origami structures presented in this thesis were designed by using the caDNAno software[96,17]. An 18-helix bundle (18HB) structure[48,62], composed by 18 parallel double stranded helices (used in papers I, II, III) and a 44 helices Hollow Brick (HB) structure (used in papers I, III), were designed with helices packed in a honey comb lattice (Figure 7a and 7b). The 2D rectangle (R) structure (used in paper III) is composed of 24 double stranded helices folded in parallel fashion (Figure 7c).

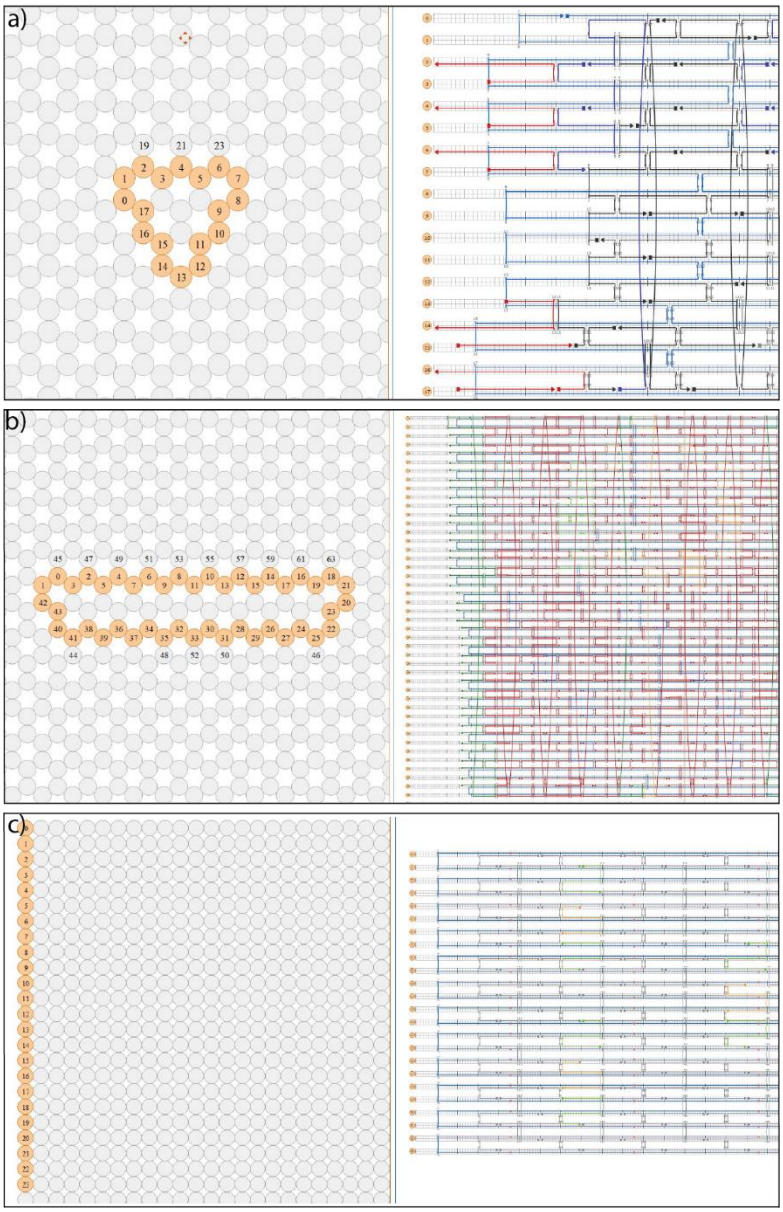

Figure 7. Design of DNA origami with caDNAno software. Representative images of structural design for a) 18-helix bundle (18HB), b) Hollow brick (HB) and c) 2D rectangle (R) structures.

The first step of designing a DNA origami was to determine the needed dimensions of the nanostructure, in order to present molecular patterns on it, in further experiments. Next, by knowing the geometrical characteristics of the B-DNA (0.34nm per base and 10.5nt for one helical turn) we designed lines with length that correspond to the length of the desired structure. These parallel lines represent the helices of the DNA scaffold that needed to be connected by crossovers. To continue, we used the "auto staple" feature of the caDNAno software, to create staple strands that connect the scaffold together. The software automatically highlighted staples that are long with thick lines, and we manually introduced staple break-points in order to create staples between 21 and 60nt. At the ends of the structures we either introduced staples that protrude by 3-5 bases (A-caps) or left unpaired scaffold to avoid aggregations during folding. We then chose randomly a point on the scaffold strand to apply the sequence of the scaffold DNA used (7560 bases for 18HB, 7246 bases for rectangle and 8634 for HB) and by using the feature "add seq" we generated the sequences of the staple strands. The staple sequences were further processed in Microsoft excel software and finalized for order.

3.1.2 Production of ssDNA scaffold

Bacterial culture of E.coli strain (JM109) starting from a single colony were grown in 2xYT media. At the exponential phase of the growth, the culture was inoculated with phages derived from M13mp18 containing ssDNA at the desired size (p7560 with 7560 bases for 18HB, p7249 with 7249 bases for rectangle and p8634 with 8634 bases for HB). The bacteria were then cultured for 4-5 hours with p7249 and p7560 phages and for 3 hours with the p8634 phages at 37oC. After this period of time, the bacteria were removed from the culture by centrifugation and the phages were isolated by PEG precipitation. The ssDNA was extracted from the phages by removing the coating of the phages with alkaline lysis followed by ethanol precipitation. The resulting pellet of ssDNA scaffold was resuspended in 10mM Tris buffer pH 8.5.

3.1.3 Folding, purification and characterization of DNA nanostructures

DNA origami structures were produced by mixing scaffold DNA with the corresponding mixture of staple oligonucleotides and subjecting the mixture to thermal annealing using a thermocycler. A standard folding reaction includes a final concentration of 20nM scaffold, 100nM of staple strands in folding buffer containing 5mM Tris, 1mM EDTA and $MgCl_2$. The optimal $MgCl_2$ concentration for each structure was determined individually in a Mg screening experiment, where different amounts of Mg were tested during the folding reaction. The presence of this divalent cation is important during folding because it stabilizes the DNA helices in close proximity, through shielding their negative charges. In the case of project II, we avoided using EDTA during the folding process because the presence of EDTA in cell experiments could activate the pathway we were studying. The complete reaction mixture was annealed on a 16 hours program (65 ^{o}C for 4min, 65 ^{o}C to 50 ^{o}C for 1 min/0.7 ^{o}C, 50 ^{o}C to 35 ^{o}C for 1h/ 1 ^{o}C, 20 ^{o}C forever).

The reaction described above contains staple strands in 5 times excess compared to the scaffold concentration and the unused material needs to be removed after the reaction is completed. In most of the experiments included in this thesis, we used an ultrafiltration method to separate the folded origami from the excess of unused staples where molecular weight cut-off filters were used (100k Amicon columns 0,5ml, Sigma, UFC5100). Initially, the filters were incubated for 10minutes at room temperature with washing buffer (1x PBS supplemented with 10mM MgCl2). The folded DNA origami was diluted with washing buffer to 400ul total

volume and transferred into the filter tube and spun down for 1 minute at 10000 rpm. This procedure was repeated until no ssDNA oligos could be detected it the flow-through, using a spectrophotometer (Nano-Drop, Thermo Fisher). The final concentration of the purified DNA origami was determined by measuring the absorbance at 260nm using Nano-drop.

The characterization of the folded DNA origami was achieved by running the structures in 2 % agarose gels (0.5x TBE, 10mM MgCl2, 0.5mg/ml ethidium bromide (EtBr)) in an ice water bath for 3 hours at 90V. The folded DNA origami shows an increased migration speed compared to the scaffold molecule on an agarose retardation assay. This electrophoretic assay can be used to detect dimers and aggregates of the DNA origami as well as non-incorporated DNA strands. The gels were imaged with ImageQuant LAS 4000 (Cytiva). To further observe the shape of the folded DNA origami, we used negative-stained transmission electron microscopy (TEM). The concentrations of the samples were adjusted to 5 or 10nM and 3 µl of samples were applied on a glow-discharged, carbon-coated, formvar resin grid for 20 seconds. The grid was then blotted on a filter paper and stained with 2% w/v aqueous solution of uranyl formate, supplemented with 20mM NaOH. The negative stained samples were imaged by Talos 120V Microscope at a magnification that is described in each experiment.

3.1.4 Solid phase synthesis of DNA origami

In this thesis we present a protocol we developed for folding DNA origami directly on a solid support. The desired amount of oligo dT25 magnetic beads (Thermo, 61005), was placed on a magnet to remove the storage buffer and was resuspended in Tris buffer (5mM Tris, 1mM EDTA). The folding mixture components (10nM scaffold, 50nM staple strand mixture, 100nM ssDNA linker and sodium polytungstate, SPT, at a final concentration of 270mM) were then added to the magnetic beads. For high folding yields we recommended to use 5.83 ng of DNA scaffold per µl of magnetic beads. The tube containing the reaction was placed in a PCR machine and folded by annealing at 65ºC for 4min, then 65 ºC to 50 ºC for 1min/0.7 ºC, 50 ºC to 35 ºC for 1h/1 ºC and 20 ºC forever until retrieved. When the reaction completed, the tube was placed on a magnet where the solution was removed and the beads were resuspended in washing buffer (1x PBS supplemented with 10mM $MgCl_2$). This procedure was repeated two additional times. Finally, the magnetic beads were resuspended in elution buffer (1x PBS supplemented with 10mM $MgCl_2$) containing the invasion strand at 250nM concentration for at least 1 hour. The tube was then placed on a magnet to separate the beads from the solution that contains the pure DNA origami.

3.1.5 Conjugation of protein with DNA

The protein Jag1Fc carrying 6x histidines (His tag) at the C terminus (used in paper II), was conjugated to a 21 bases oligonucleotide. Initially, the protein was buffer exchanged to 1x PBS pH 6.3, and 20 times excess in molar concentration of the chemical Bis-sulfon-PEG4-DBCO was added for 4 hours at room temperature (RT) (Figure 8). This chemical reacts with two imidazole rings of the His tag resulting in a protein carrying a DBCO group. Then we used desalting columns (Thermo Fisher, Zeba spin desalting columns 7k) to buffer exchange the protein in 1x PBS pH 7.2 and remove the unreacted excess of the chemical compound. The DBCO modified Jag1 protein was reacted with a 21 bases long N3-modified oligonucleotide in a coper free click chemistry reaction for 4 hours at RT. The excess of oligonucleotides were

removed with weight cut-off filters (50k Amicon columns 0,5ml, Sigma, UFC5050). The protein modified with DNA oligos was diluted with washing buffer (1x PBS) to 400ul final volume and placed in the filter tube and spun down for 2 minute at 14000 rpm. This procedure was repeated until no ssDNA oligos could be detected at the flow-through using a spectrophotometer (Nano-Drop, Thermo Fisher). The final concentration of the protein conjugated with DNA was measured by Bradford assay (Sigma, B6916-500ml).

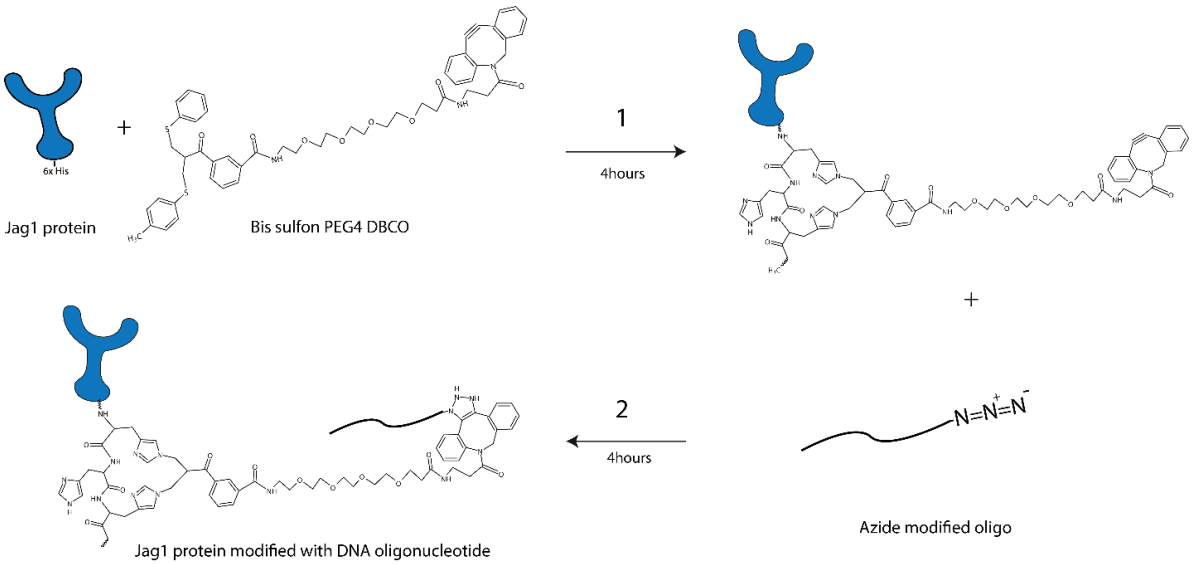

Figure 8. Conjugation reaction of Jag1Fc protein with single stranded DNA oligonucleotide. Initially, the protein was mixed with the chemical compound Bis-Sulfon-PEG4-DBCO that selectively reacts with imidazole groups of His-tag present at the C terminus of the protein (1). DBCO modified protein reacted with an azide modified oligo at a Cu-free click chemical reaction to form protein-oligonucleotide conjugates (2).

3.1.6 Formation and purification of functionalized DNA origami

In this thesis, two approaches were used to functionalize DNA origami. In the first strategy, a modified oligonucleotide was added directly during the folding process. Such modifications are probes used in paper I (digoxigenin, 4-hydroxy-3-iodo-5-nitrophenylacetate, 4-hydroxy-3-nitrophenyl) and fluorophores in paper II and III. These modifications can survive the high temperatures used during folding process. In the second strategy, we introduced modifications that are not resistant to high temperatures, such as proteins. In this case the DNA origami was folded with an oligonucleotide protruding outside of the structure, which is complementary to the protein-DNA conjugate sequence. The DNA origami with protruding oligos, after purification with ultrafiltration, were incubated with the protein conjugates at 37 ^{o}C for one hour, followed by a rapid cooling to 22 ^{o}C and incubated at the same temperature for 14 hours.

Purification of functionalized DNA origami was performed with different methods. When the modification was added during folding and its molecular weight was below 100kDa, removal was achieved with ultrafiltration procedure after folding. When the protein Jag1Fc was added to the DNA origami (paper II), successful removal of the excess of the protein was achieved with size exclusion purification (FPLC, Superose 6 column). In the solid phase synthesis protocol we present in this thesis, we were able to remove any modification we introduced on the structure regardless of the molecular weight with our solid support (paper III).

3.1.7 Surface Plasmon resonance (SPR)

Surface Plasmon Resonance is a label free technique able to measure the affinity of interaction and determine the association and dissociation rates between molecules. Association and dissociation are measured in arbitrary units, called Response units (RU), represented in a sensorgram. During the measurement, one of the components is immobilized on a chip surface while the other interactant is passed over the surface.

In our experiments we took advantage of the strong interaction between streptavidin and biotin, to immobilize our biotin modified ligands on the chip surface. The CM3 chip surface was first activated with NHS/ECD (N-hydroxysuccinimide/1-ethyl-3-(3-dimethylaminopropyl) carbodiimide) to subsequently immobilize streptavidin at 10μg/ml in 10mM Sodium Acetate buffer pH 4.5 at a 6 minute contact time and 10 μl/min flow rate.

In paper I we used the SPR technique to measure the binding kinetics of antibodies when precise patterns of antigens, presented on a DNA origami, were immobilized on a chip surface. Firstly, 200nM of a biotinylated oligonucleotide diluted in 1xHBS-EP running buffer, was injected over the streptavidin surface for 20 minutes with a flow rate 10 μl/min followed by a washing step with 50mM NaOH for 5 minutes. The DNA origami carrying antigen patterns on one side and ssDNA on the opposite side, were injected over their complementary biotinylated oligo previously anchored on the chip surface, with a flow rate 2 μl/min for 20 minutes. A washing step with buffer for 10 minutes removed any non-specifically bound DNA origami. Antibodies were diluted to five increasing concentrations close to a range of its KD (0.025-0.5 nM for anti-DIG antibodies, 1-50 nM for anti-biotin antibodies and 0.0256-1nM for anti-NIP antibodies), and injected from the lowest to highest concentration for 5 minute each, with a flowrate 30 μl/min, followed by a 15 minute dissociation step. All antibody kinetic experiments with DNA origami antigen patterns were performed in 1xHBS-EP buffer supplemented with 10mM $MgCl_2$ and after each cycle the surface was regenerated with a 5 minute injection of 50nM NaOH. The antibodies were injected using single cycle kinetics experiment and the binding curves were fitted to a 1:1 Langmuir binding model with the T200 evaluation software, to calculate the association rates, dissociation rates and binding affinities. The experiments were performed with a BIAcore T200 instrument.

In paper II we used SPR measurements to show the different binding affinities of several Jag1 nanopatterns with Notch1 receptor. The biotinylated extracellular domain of the human Notch1 receptor (8-12 EGF) was immobilized at 200 RU. Jag1Fc DNA nanopattern samples were diluted to concentrations ranging from 2,5 nM to 10 nM in PBS, pH 7.4, supplemented with 10 mM $MgCl_2$. The flow rate of the samples was adjusted to 10 μl/min, and a total amount of 70 μl was injected for 120 seconds on the immobilized receptor and multi-cycle kinetics experiment was performed. After the injection, the sample was left to dissociate by injecting buffer and at the end of each cycle, MgCl2 buffer was used to regenerate the surface for 60 seconds at 30 μl/min flowrate. Data were processed with the BIAevaluation 3.2 software using a 1:1 Langmuir binding model.

3.2 BIOLOGICAL ASSAYS

3.2.1 Culture of mammalian cells

The mammalian cells cultured in the work presented in this thesis were HEK293T cells for Jag1 protein production and human derived induced pluripotent stem (iPS) cells for the investigation of Notch signaling pathway (Nes, AF22) (paper II)

HEK293T cells were cultured in DMEM (Dulbecco's modified eagle medium) supplemented with 10% FBS (Fetal bovine serum) and 1% penicillin and streptomycin (pen/strep). The cells were cultured in flasks T75 (VWR, 734-2313) and expansion was performed when cells reached 90% confluency. For each round of high scale protein production 30 flasks were used. When cells were in 90% confluency, we transfected them with Jag1 plasmid. We pre-mixed Jag1 plasmid and transfection reagent (lipofectamine 2000) at a ratio 1:3 in optimem media, let the complex form for 15 minutes and then added it into the cells. One day after transfection media were collected, and fresh DMEM with FBS and pen/strep were added to the cells for 4 more days. The total amount of media collected from day1 and day5 were further processed for protein purification by using the affinity purification column His trap FF. The Jag1Fc protein that we produced contains 6 Histidines at the C terminus which was used for capture on a precharged Ni Sepharose 6 Fast Flow column by immobilized metal ion affinity chromatography (IMAC).

NES cells were cultured as adherent cells in cell culture flasks (VWR, 734-2311) previously coated with 20 μg/ml polyornithine (Sigma) for 1 hour and 1 μg/ml Laminin2020 for 4 hours (Sigma). Cells were cultured in NES culture medium DMEM/F12+GlutaMax (Gibco), supplemented with 10 μl/ml N-2-supplement (100×, Thermo Fisher Scientific), 10 μl/ml Penicillin-Streptomycin (10,000 U/ml, Thermo Fisher Scientific), 1 μl/ml B27-supplement (50×, Thermo Fisher Scientific), 10 ng/ml of bFGF (Life Technologies) and 10 ng/ ml of FGF (PeproTech). The culture medium was replaced every second day. The NES cells were passaged enzymatically at 100% confluency using Trypsin-EDTA (0.025%, Thermo Fisher Scientific). NES cells were seeded at a density of 40,000 cells/cm^2. For the cell stimulation experiments we used 96 well plates where cells were seeded for 6 hours followed by 3 hours stimulation with Jag1 DNA nanopatterns.

3.2.2 RNA extraction

Two different protocols for RNA extraction were followed in paper II, for detection and characterization of the Notch signaling pathway. All samples analyzed with qPCR experiments were RNA extracted with the Power Sybr Green Cells-to-Ct Kit (Thermo Fisher Scientific, 4402954). This protocol is optimal for working with 10 to 10^5 cells per reaction. Media from adherent cells were removed and 50 μl of Lysis solution were added to each well, pipetted for 5 times and incubated at room temperature for 5 minutes. Stop solution at 5μl was then added to the solution, pipetted for 5 times and incubated at room temperature for 2 minutes. In the same Kit reagents for reverse transcribing (RT) the mRNA to DNA were included. The reaction mixture for the RT reaction contains 25 μl 2x Sybr RT buffer, 2.5 μl 20x RT enzyme mix, 12.5 μl water and 10 μl of the extracted RNA sample. The reaction was added into a thermocycler

and incubated at 37ºC for 60 min followed by RT inactivation at 95 ºC for 5 min. The samples were hold at 4 ºC and stored at -20 ºC till the qPCR reaction.

The samples analyzed with mRNA sequencing experiments were RNA extracted by using the RNeasy Micro Kit (Qiagen, 74004). This Kit is also suitable for working with less than 10^5 number of cells in a 96 well plate set up. RNA molecules longer than 200 nucleotides are purified which means that this procedure enriches mRNA extraction while smaller RNAs (such as 5.8S rRNA, 5S rRNA and tRNAs, which together make up 15–20% of total RNA) are excluded. Media from adherent cells were removed and 75 µl Buffer RLT was added, pipetted up and down to disrupt and lysate the cells. Sample was transferred to a microcentrifuge tube and 75 µl of 70% ethanol were added. The samples were then transferred to MinElute spin column and centrifuged for 15 seconds (sec) at 8000g to bind RNA on the column. The samples washed with 700 µl Buffer of RW1, with 350 µl Buffer of RW1 and 500 µl Buffer of RPE and centrifuged after each wash for 15 sec at 8000g. After these steps, 500 µl of 80% ethanol were added and centrifuged for 2 min at 8000 g and at maximum speed for 5 minutes with the tube's lid open. The RNA was then eluted with 14 µl RNase-free water and centrifuged for 1 min at full speed. The samples were further processed for library preparation with the TruSeq stranded mRNA Kit (Illumina, 20022371).

3.2.3 Real time qPCR

The real time quantitative polymerase reaction technique is used for the amplification and detection of targeted DNA molecules. The two existing methods for detection in real-time PCR use either a non-specific fluorescent dye that intercalates to double strand DNA (Sybr Green) or a sequence-specific DNA probe that is labelled with a fluorescent reporter, which allows detection only after hybridization with the complementary target sequence. In the sequence specific method, the probe carries a fluorophore on one side and a quencher on the other side. The primer sequences initiate the DNA polymerase reaction, and when it reaches the probe sequence, its exonuclease activity degrades the probe, allowing the fluorophore to be excited by the laser. All RT-qPCR experiments presented in this thesis were performed with a Step-One-Plus real time PCR machine (Applied Biosystems) using the StepOne Software v2.3.

In paper II we used the Power Sybr Green Cells-to-Ct Kit which is using a Sybr Green dye for detection. The reaction mixture included 10 µl of Sybr Green, 1 µl of primers (250nM final concentration), 5 µl of water and 4 µl of cDNA. Primers used in this study are Hes1 Fw: AGG CGG ACA TTC TGG AAA TG, Hes1 Rev: TCG TTC ATG CAC TCG CTG A, GAPDH Fw: ACT TCA ACA GCG ACA CCC ACT and GAPDH Rev: CAC CCT GTT GCT GTA GCC AAA. The reactions were placed into the qPCR machine and cycled using the following program: Enzyme activation at 95oC for 10 min, 40x PCR Cycles of 95oC for 15 sec and 60oC for 1 min, followed by a melting curve.

In paper IV, presence of SARS-COV2 genes in samples were detected by reverse transcription and qPCR using the TaqPath RT-qPCR master mix (Thermo, A15299). The total reaction was 20µl and contained 5 µl TaqPath master mix, primers-probe mix, sample, and RNase free water. The concentrations of primers and probes were: E and RdRP: 300 nM each primer, 200 nM probe; N1 and RdRP: 500 nM each primer, 125 nM probe. The thermal annealing steps

were: 25 °C for 2 min, 50 °C for 15 min, 95 °C for 2 min, and 45 cycles of 95 °C for 3 s and 56 °C for 30 s.

Table 1. Primers and probes used for SARS-CoV-2 RT-qPCR.

Name	Amplicon length (bp)	Description	Sequence (5' to 3')
N1	72	Forward	GACCCCAAAATCAGCGAA AT
		Reverse	TCTGGTTACTGCCAGTTGAATCTG
		Probe	**FAM-** ACCCCGCATTACGTTTGGTGGACC -**BHQ1**
E	113	Forward	GGAAGAGACAGGTACGTTAATA
		Reverse	AGCAGTACGCACACAATCGAA
		Probe	**FAM-** ACACTAGCCATCCTTACTGCGCTTCG-**BHQ1**
RdRP	81	Forward	GTCATGTGTGGCGGTTCACT
		Reverse	CAACACTATTAGCATAAGCAGTTGT
		Probe	**FAM-** CAGGTGGAACCTCATCAGGAGATGC**- BHQ1**
RNase P	65	Forward	AGATTTGGACCTGCGAGCG
		Reverse	GAGCGGCTGTCTCCACAAGT
		Probe	**FAM-** TTCTGACCTGAAGGCTCTGCGCG-**BHQ1**

3.2.4 Ethical considerations

In paper IV we intended to create a clinical method for detection of SARS-COV2 virus. This study was performed according to the Swedish Act, concerning the Ethical Review of Research Involving Humans. Ethical oversight and approval were obtained by the appropriate Swedish Authority (Dnr 2020-01945, Etikprövningsnämnden). The clinical samples were collected and deposited in transport medium (Virocult MED-MW951S, Sigma; Transwab MW176S, Sigma; or Eswab 482 C, COPAN) at the Karolinska University Hospital, Stockholm, Sweden. In this work we used anonymized or pseudo-anonymized surplus material from samples that had been collected for clinical diagnostics of SARS-CoV-2, in accordance with the Swedish Act concerning the Ethical Review of Research Involving Humans which allows development and improvement of diagnostic assays using patient samples, which were collected to perform the testing in question. Informed consent was obtained from the participants.

4 RESULTS AND DISCUSSIONS

4.1 PAPER I

4.1.1 Introduction of the PSPR technique

In paper I we introduced a new method to measure the spatial tolerance of antibodies, by using precise nanoscale patterns of antigens displayed on a DNA origami nanostructure, with a surface plasmon resonance (SPR) instrument. A streptavidin coated chip surface was modified with biotinylated oligonucleotides which serve as anchors for the antigen decorated DNA origami carrying complementary ssDNA oligos (Figure 9). Two different types of nanostructures were used in this study: an 18 helix bundle (18HB) rod like structure and a 44 helices brick like structure. Increasing concentrations of different antibodies were flown over the immobilized antigen patterns in a single cycle kinetics experiment and binding kinetics for several antibodies over antigen distances were measured (Figure 9). This method uses immobilized patterns with SPR technique and for this reason we refer to it as PSPR (patterned SPR).

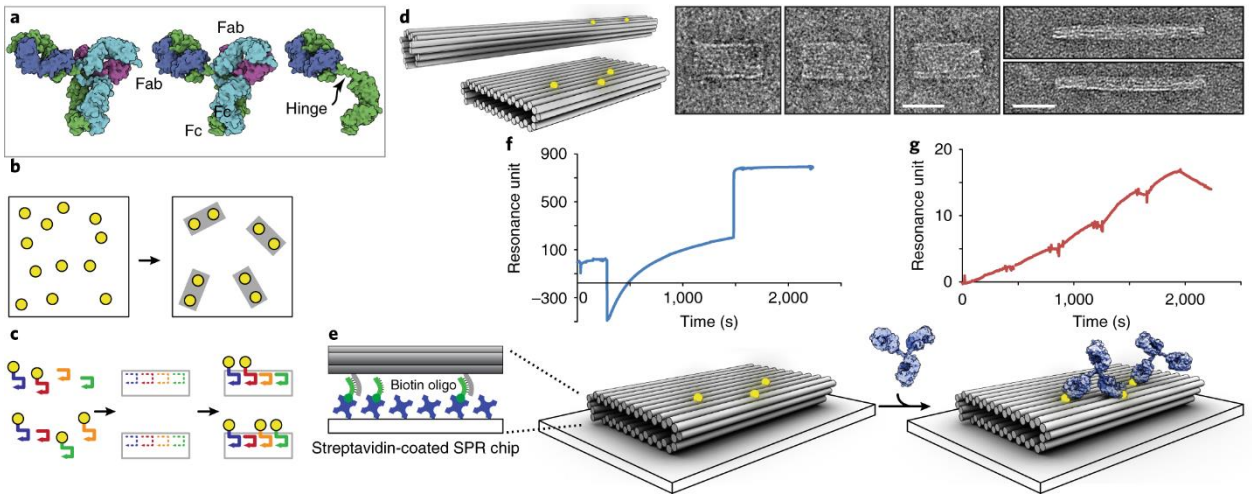

Figure 9. The PSPR method. a, Three-dimensional (3D) rendering of human IgG1 based on X-ray crystallography data (Protein Data Bank PDB:1HZH). **b**, The advantage of PSPR: in contrast to conventional SPR (left), which randomly arranges its ligands on the surface, the PSPR method (right) utilizes DNA origami to prepattern the antigen of interest (yellow dots) prior to immobilization. **c**, Antigen nanopatterns were fabricated using different combinations of antigen-decorated staple oligonucleotides (differently coloured lines). **d**, 3D models using cylinders as a representation of double helices (left) and transmission electron microscopy negative-stain micrographs (right) of the DNA nanostructures used in this study. Scale bars, 40 nm. Two types of DNA nanostructures, an 18-helix rod and a 44-helix brick, were used to pattern the antigens. **e**, The antigen nanopatterns were immobilized onto a streptavidin-biotinylated oligonucleotide surface via oligonucleotide hybridization to sequences that protrude from the bottom of the origami. **f**,**g**, These were first allowed to immobilize in the SPR machine (**f**), followed by an injection of increasing antibody concentrations and finally a dissociation phase (**g**). The kinetic data can be obtained by fitting the binding curves with a 1:1 binding model. The model shows the origami and antibody rendered to scale, and illustrates a 16 nm bivalent binding and a monovalent binding.

4.1.2 Measuring the spatial tolerance of human antibodies

To explore the flexibility of the four human IgG subclasses (IgG1, 2, 3, 4), we used the 18HB DNA origami decorated with two 4-hydroxy-3-iodo-5-nitrophenylacetate (NIP) antigens at various distances from 3-44nm and a single antigen decorated nanostructure (0nm). When we placed two antigens on the nanostructure we observed a decrease in the Kd compared to the

single antigen sample. Among them, the binding was weaker when the antigens were separated by 3 and 17nm and the maximum affinity was observed at 16nm distance (Figure 10).

The different IgG subclasses are known to differ in the flexibility of their hinge regions. IgG 1 and IgG4 show similar flexibility, IgG2 is the stiffest among them, while IgG3 is the most flexible. In our SPR measurements we also observe differences in the binding affinities between the IgG subclasses. More specifically, IgG1 and IgG4 showed similar behavior, while IgG2 showed a slower increase of affinity at short distances, but became stronger at 14-16nm distances. IgG3 which is the most flexible, showed a strong binding even at short distances.

To further explore the effect of the hinge region on the binding affinity of the IgG3 subclass, we engineered the IgG3 antibody to have a shorter 15 amino acids hinge region (m15), a 5 amino acids hinge region (HM5) and created a variant lacking completely the hinge region (HM4). Surprisingly, the HM4 mutant exhibited a similar behavior to IgG2, whereas the m15 mutant showed a similar binding behavior to IgG1 and IgG4. We also engineered a monomeric IgM variant which doesn't form pentamers or hexamers like the natural IgM. This antibody that doesn't contain a hinge region but it has an extra constant Fc domain, showed a strong bivalent binding for all distances tested between 3 to 17nm. Stronger binding was observed even at 29nm which indicates that the monomeric IgM either is able to stretch, because of partial unfolding, or it multimerizes to reach long distances.

These results were further explored by using antibodies with higher and lower affinities to their cognate antigens compared to anti-NIP antibodies. A monoclonal rabbit anti-DIG antibody was used to measure the binding kinetics to Digoxigenin antigens presented on a DNA origami structure using our PSPR technique. When the structure had one antigen present (0nm) the Kd was between 25-35pM while when we placed two Dig antigens in close distance (7 and 14nm) a tenfold change increase was observed in the binding affinity. In contrast, when we studied the human IgG 1 and 3 and their binding tolerance against the lower affinity 4-hydroxy-3-nitrophenyl (NP) antigens, a much lower affinity was observed at 3,7,14 and 17nm, which indicates that the antibody fails to bivalently bind at these distances, but a sharp increase at 16nm distance indicates a stronger bivalent binding.

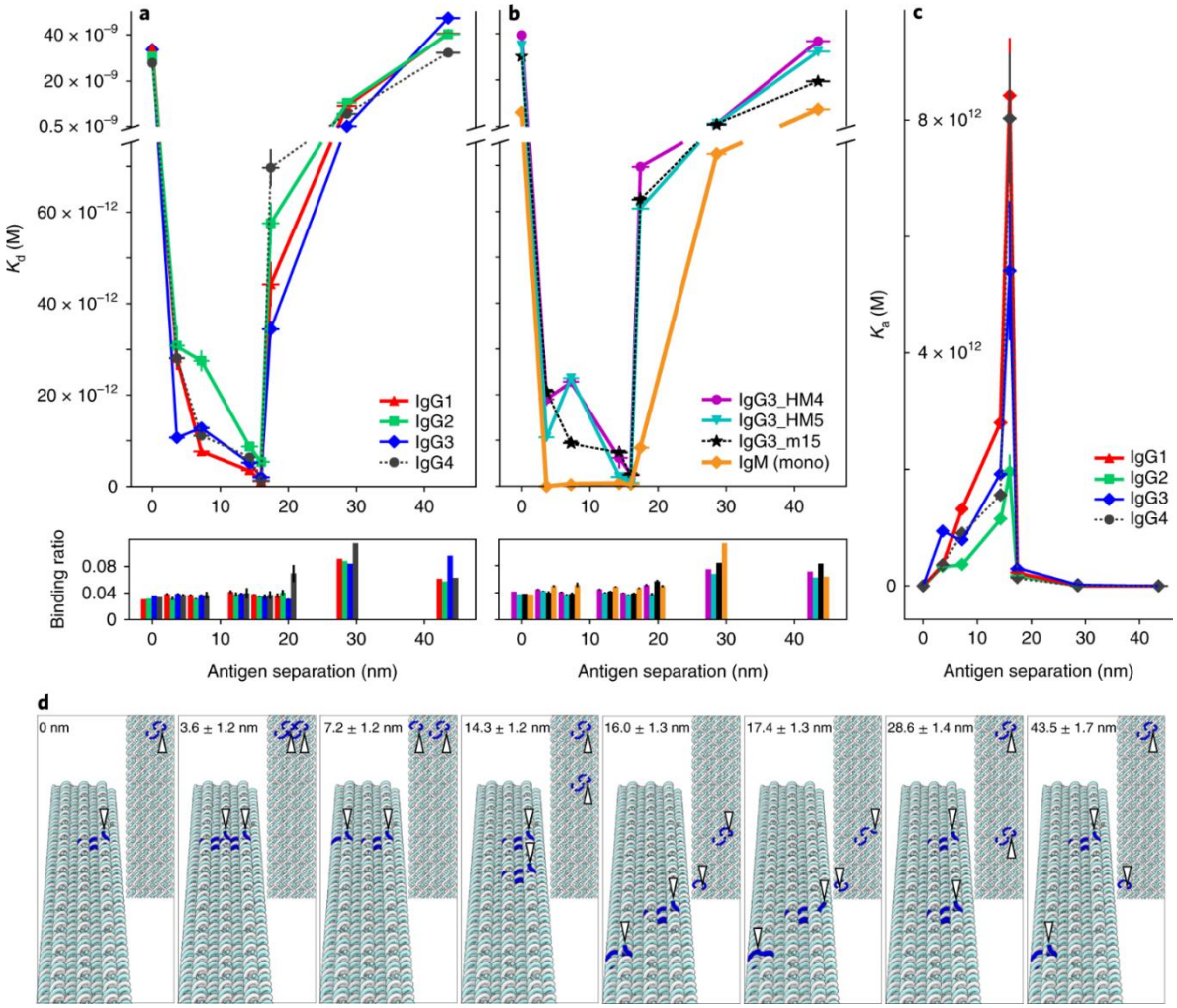

Figure 10. Antibody binding to precise antigen separations. Human anti-NIP antibodies binding to two NIP molecules patterned on the 18HB at varying separations. **a,b**, Scatter graphs of K_d and binding ratio (maximum resonance unit (RU) of antibodies/RU of nanostructures, which corresponds to average antibodies per structure) for the various separations. Exact structure designs are given in **d**. The '0' distance is just one displayed antigen. The *y* axis (top panels) shows the apparent binding affinity recorded and fitted with BIAcore t200 evaluation software. The amount of antibody (in RU) that is bound to 1 RU of the structure (the binding ratio) is plotted in the bottom panels. **a**, Data for all wild type IgG subclasses. **b**, Data for IgG3 hinge mutants and monomeric IgM. *y*-axis error bars = s.e.m., **c**, The same data as in **a** plotted as association constants, K_a (= $1/K_d$), versus separations for the IgG subclasses. A peak behavior in the changes of K_a was observed for all the tested antibodies, the bivalent binding becomes weaker at short (3–7 nm) and long (17 nm) distances, and this behavior varies between different antibody subclasses ($n = 3$ or 4); central values = average value). **d**, Illustrations (top (left) and perspective (right) views) of the 18HB show the locations of the NIP-modified staple-oligonucleotides in blue and the NIP locations highlighted with white arrowheads. The distances are shown as the design distance ± distance error calculated.

4.1.3 Validation of antigen decorated DNA origami

The quality control of folded DNA origami nanostructures, used on PSPR measurements, was assessed by Transmission Electron Microscopy (TEM) (Figure 11a and 11e) and gel retardation assays (Figure 11b, c, d, f). To validate whether the different binding affinities, previously observed, are due to the flexibility of antibodies and their binding affinity to the cognate antigens, we performed gel retardation assays with the antigen decorated DNA origami. Initially, we observe that all DNA nanostructures decorated with antigens at various distances were folded at the same quality (Figure 11b). When we incubated the 0-17nm structures with 2000 times excess of anti-NIP human IgG1 we observed that the structures run at lower speed than the empty structure while on 0nm (monovalent binding) there is no observable difference

at the migration speed (Figure 11c). For the distances 29 and 44nm we added 4000 times excess of antibodies, but a similar migration speed was observed as with the 0nm structures. This result shows that when the binding affinity is in the nM range it is difficult to see migration changes with gel retardation assay for the monovalently bound structures. To confirm this hypothesis, we ran the same experiment but the DNA nanostructures were decorated with the Dig antigens and the samples were incubated with the monoclonal rabbit anti-DIG antibody (Figure 11d). In this case that the affinity of the antibody is at the pM range, we observed the same shift between 0 and 17nm which means that monovalently bound antibody showed the same migration while 29 and 44nm migrate even slower which could correspond to two antibodies monovalently bound on the DNA origami. These results in combination show that an undetectable amount of nanostructures had defects in antigen oligonucleotide incorporation and the SPR results showing differences in binding affinities are due to the different response of antibodies to the antigen patterns.

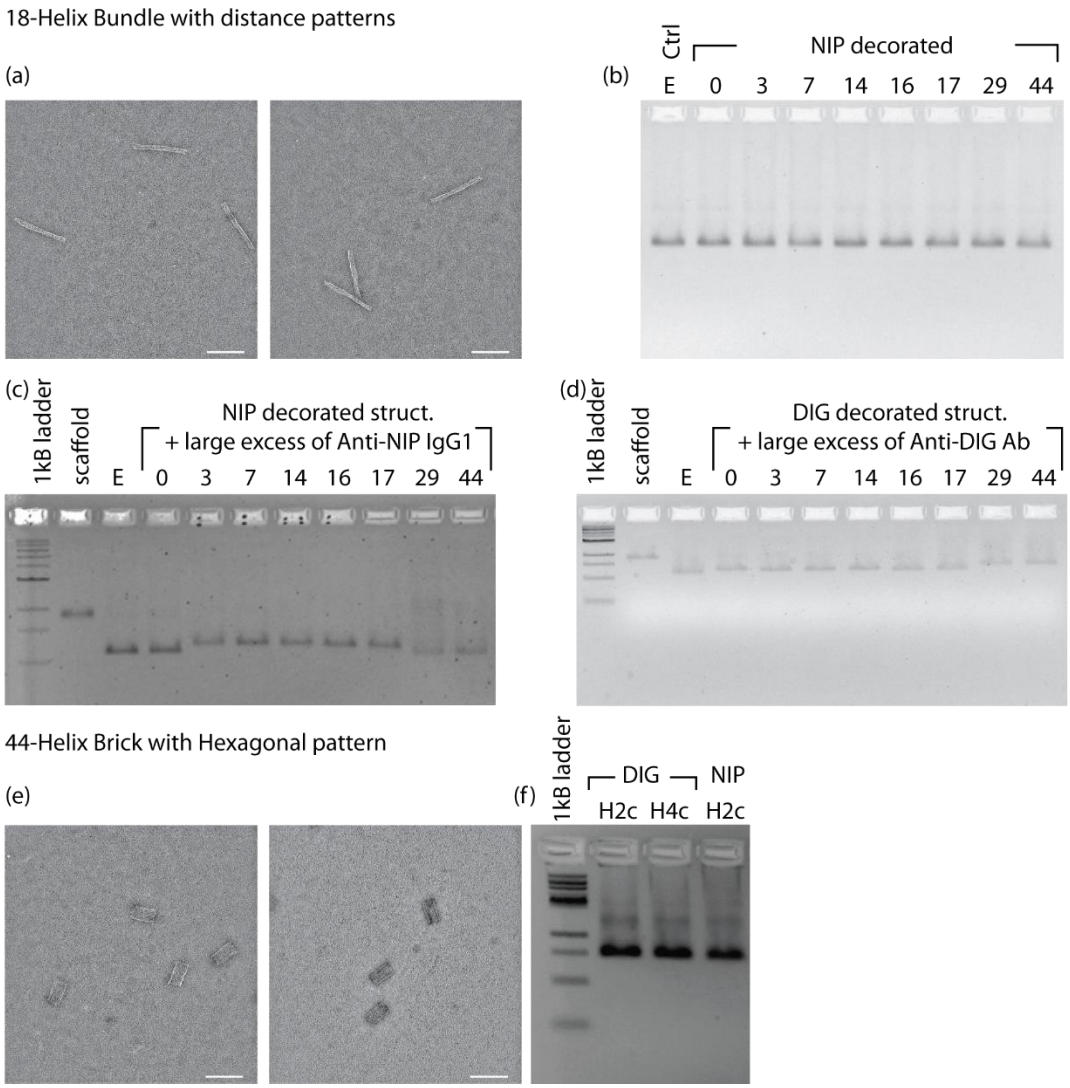

Figure 11. Quality control of utilized structures. Transmission Electron Microscopy (TEM) (a),(e) and gel characterization (b),(c),(d) and (f) of the distance displaying 18-helix bundle and hexagon displaying brick nanostructures. All gels are 2% agarose, pre-stained with Ethidium Bromide (EthB) (a) and (e): Uranyl Formate negatively stained TEM of E ('Empty' *i.e.* bearing no sites) control structures structures. Scale bars are 100 nm. (b) Identical gel mobility of the distance displaying 18-helix bundle reveals no discernable difference between the distance cases indicating proper folding of all structures. Empty, E, structure bearing no protruding sites. Other lanes are the structures used for the NIP distance experiments. (c) Structures used for the NIP distance experiments

incubated with an excess (1:2000 structure:Abs 0-17 nm, 1:4000 29 & 44 nm) of anti-NIP human IgG1. Appreciable binding and resulting shift can be seen in the samples showing bivalent binding (3-17 nm) whereas the samples showing predominantly monovalent binding (0, 29 and 44 nm) display barely discernable shifts due to the low affinity of monovalent binding.(d) Using the higher affinity rabbit anti-DIG Abs with DIG decorated structures reveals shifts also for the monovalent samples (0, 29 and 44 nm) with a larger mobility shift for the longer distances (29 and 44 nm) indicating two monovalently bound Abs. Excess is 1:1000 structure:Abs 0-17 nm, 1:2000 29 & 44 nm. (f) Agarose gel of the hexagonal pattern displaying brick structures without Abs showing no discernable differences in folding quality.

4.2 PAPER II

4.2.1 Characterization of Jag1 nanopatterns (JNPs)

In paper II we used nanoscale patterns of DNA origami decorated with Jag1 ligands, to study the effect of ligand clusters on the activation of Notch signaling pathway. Specifically, we used a rod like DNA origami structure to precisely position one, two, three, four or eight Jag1Fc proteins. To achieve this, the proteins were conjugated to a 21 bases oligonucleotide, which was used for the hybridization reaction to its complementary oligo protruding from the DNA origami. The successful hybridization reaction was confirmed with gel retardation assay, where an increased shift was observed when more proteins were loaded on the DNA origami (Figure 12B). Negative stain transmission electron microscopy (TEM) was used to observe the correct geometry of the rod like structures (Figure 12C). The apparent KD of different Jag1 nanopatterns (JNPs) was measured with surface plasmon resonance (SPR) instrument where the extracellular part of Notch receptor was immobilized on the chip. By performing multi-cycle kinetics with increasing concentrations of JNPs, we observed that the affinity increased when the number of the proteins per nonpattern increased (Figure 12D). To further validate the number of Jag1 proteins incorporated per nanopattern, we used TIRF and DNA-PAINT imaging to show the functionalization state of each JNP. DNA origami structures were prepared with biotin handles for immobilization in the imaging chamber and the proteins were conjugated to a longer oligo carrying DNA-PAINT docking sites, for detection of the proteins on the structures with DNA PAINT imaging (Figure 12E). From this experiment we observed that for all the structures the fraction with the highest detected frequency was the one with the designed number of proteins (Figure 12F).

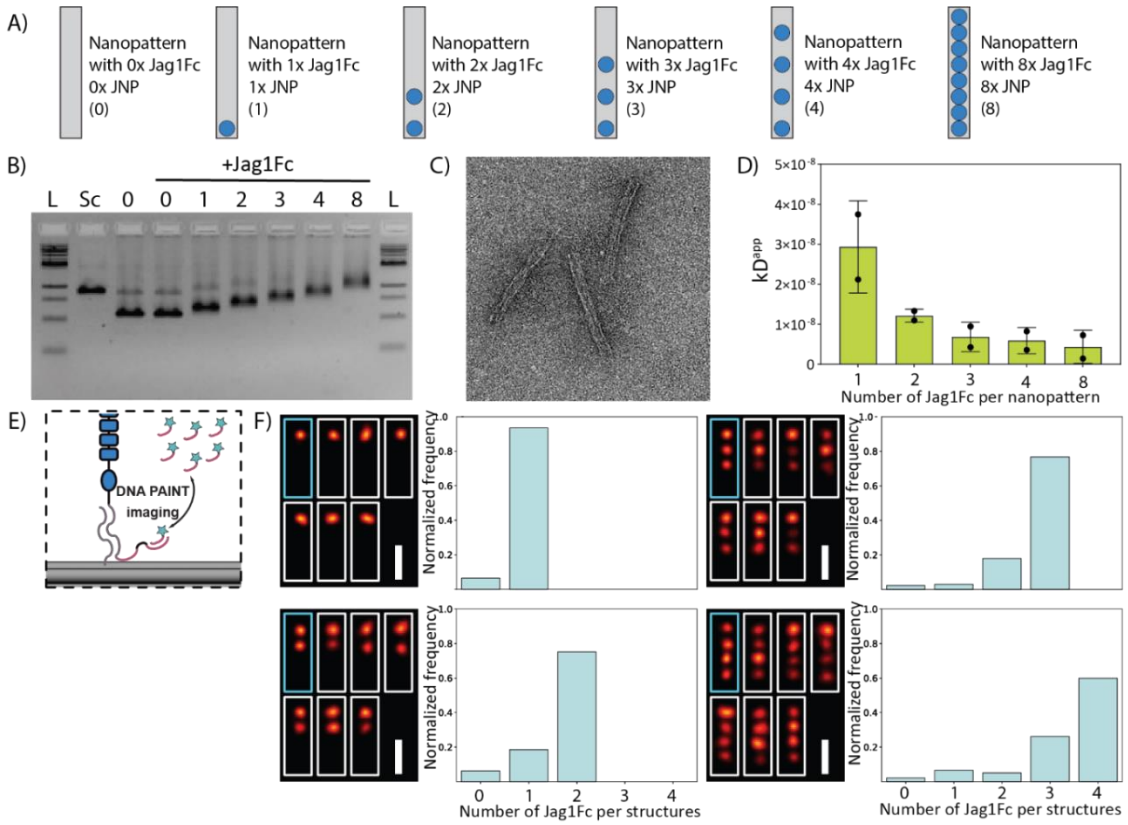

Figure 12. Characterization of Jag1Fc DNA nano-patterns. A) a rod like DNA origami was used to create 1x, 2x, 3x, 4x and 8x Jag1Fc nanopatterns (JNPs). B) Gel retardation assay reveals an increasing shift of DNA when increasing number of proteins positioned on top of the DNA origami. 1Kb ladder (L), scaffold (Sc), 0x JNP (0), 1x JNP (1), 2x JNP (2), 3x JNP (3), 4x JNP (4) and 8x JNP (8) run on agarose gel stained with ethidium bromide. C) Negative stained TEM of DNA origami rod D) Surface Plasmon Resonance measurements when Notch1 (EGF8-12) receptor immobilized on chip surface and increased concentrations of 1x JNP (1), 2x JNP (2), 3x JNP (3), 4x JNP (4) and 8x JNP (8) flow through the chip. The mean apparent kD of different Jag1Fc nano-patterns is shown on a bar plot where dots represent two individual experiments. E) Schematic representation of the DNA origami used for the DNA PAINT experiments with Jag1 proteins conjugated to DNA-handles containing a pair of DNA-PAINT docking sites used for protein detection (red). F) Average (cyan) and individual cropped DNA PAINT images of nanopatterns containing 1 Jag1Fc (0 Jag: 6.5%, 1 Jag: 93.5%, N: 849), 2 Jag1Fc (0 Jag: 6.2%, 1 Jag:18.6%, 2 Jag: 75.2%, N: 512), 3 Jag1Fc (0 Jag: 2.2%, 1 Jag: 3.0%, 2 Jag: 18.0%, 3 Jag: 76.8%, N: 935) and 4 Jag1Fc (0 Jag: 2.1%, 1 Jag: 6.6%, 2 Jag: 5.1%, 3 Jag: 26.2%, 4 Jag: 60.0%, N: 470) (scale bar = 50nm) with the bar graphs showing the Jag site occupancy distributions of the different nanorods

4.2.2 Activation of Notch signaling pathway with JNPs

To test that JNPs can activate the Notch signaling pathway, we used an iPS cell line which shows high Notch activity. We performed immunostaining with an antibody against the extracellular part of Notch1 to confirm the presence of Notch1 receptor. To compare the effect of different Jag1 patterns and not Jag1 quantities on the Notch activation, we normalized the JNP concentration to the total amount of proteins. Then we stimulated the cells with the same concentration of proteins displayed on different nanopatterns and performed RNA extraction and RT-qPCR analysis with primers against a specific to the Notch pathway gene, Hes1, and an endogenous gene, GAPDH. This experiment showed significant upregulation of Hes1 gene when more than one protein was placed per nanopattern. We further validated our result by performing proximity ligation assay (PLA) experiment, using an antibody against a region of the intracellular part of Notch receptor that is exposed after cleavage from γ-secretase. Cells were stimulated with empty nanostructures (showing the endogenous levels of Notch activity) and a nanostructure that is decorated with 8 Jag1 proteins (8x JNP). With this experiment we

observed on the microscope more PLA signal per cell when we stimulated with the 8x JNP compared to empty nanostructures. In order to explore the effect of different JNPs on gene expression levels, other than Hes1, we performed mRNA sequencing analysis. We stimulated cells with empty nanostructures (resembles the endogenous activity levels of genes), a DNA origami containing 1 Jag1Fc (1x JNP) and a DNA origami with 8 Jag1Fc (8x JNP), RNA was then extracted and mRNA libraries were prepared for each sample in triplicates. Using a heat map analysis, many genes were observed to be upregulated by each condition and many of them were recognized as Notch pathway related genes. All the results from these experiments, show successful activation of Notch pathway by Jag1 nanopatterns displayed on DNA origami and particularly when we form bigger clusters of Jag1 ligands.

4.2.3 Exploring the activation mechanism of Notch signaling pathway by JNPs.

The ligand induced activation mechanism of Notch pathway requires the exposure of the NRR region to the ADAM10 metalloproteases and the subsequent cleavage by γ-secretase. The prevailing hypothesis for the NRR exposure involves forces generated by endocytosis of the ligand-receptor complex induced by a neighboring ligand expressing cell. Forces induced by magnetic beads has also been shown to induce cleavage of the extracellular part. Although in our Jag1 nanopattern system we don't introduce external forces, we would like to investigate if there are repulsion forces generated by the negative charged surface of the DNA origami to the negative charged cell membrane that could cause the observed receptor activation. For this purpose we coated the external surface of the DNA origami with oligolysine solution (K10) at a ratio 0.5:1 N:P which was previously shown to not aggregate the structures[55]. We stimulated iPS cells with bare JNPs and JNPs coated with K10 and measured the activation of the Notch pathway, where the same activation levels were observed between the two conditions. The extracellular cleavage of Notch can be facilitated either by ADAM10 when is ligand dependent or by ADAM17 when is a ligand independent activation. In order to assure that we stimulate the pathway by a ligand dependent mechanism we used a selective inhibitor of ADAM10. Prior to cell stimulation the inhibitor GI 254023X was added to the cells. Seven wells containing different concentrations of inhibitor and one well without inhibitor were stimulated with the same concentration of 4x JNP. RNA was extracted and qPCR experiment with primers for HES1 and GAPDH revealed decreased activation of Notch pathway when the concentration of inhibitor was increased. Specifically, the IC50 was calculated to be 1,7nM which indicates a selective inhibition of the ligand-receptor interaction.

We hypothesized that Jag1 clusters activate the Notch pathway, because they increase the local stability of the ligand-receptor complex through multivalent interactions. To validate this hypothesis, we produced Jag1 nanopatterns decorated with cholesterol moieties at the sides of the structure, which facilitate as anchors to the cell membrane. We then stimulated iPS cells with those structures and showed increased activation of Notch pathway by measuring Hes1 gene levels, compared to structures without cholesterol moieties. From this result we conclude that prolonged residence time helps the complex accomplish a successful interaction. This prolonged interaction was observed with microscopy imaging when structures carrying fluorophores appeared to interact more with the cells.

To verify that Notch activation depends on local avidity increase, induced by clusters of ligand, we produced a nanopattern that was decorated with Jag1 and a protein that interacts with integrin receptors and CD36. It has been previously described that integrins co-localize with Notch1 in neural progenitors. This nanopattern which contains on one position a Jag1 protein and on three positions the protein Bai1, is similar to the nanostructure decorated with 4 Jag1 proteins. Surprisingly, the DNA origami displaying the combination of Jag1 and Bai1 proteins gave the same activation of Notch pathway compared to a structure decorated with 4 Jag1 proteins (4x JNP). This result supports further our hypothesis that Notch activation requires prolonged ligand binding which can be achieved in a biologically relevant context by ligand clusters through their increased avidity.

4.3 PAPER III

4.3.1 Introduction of the solid phase synthesis of DNA origami technique

In paper III we introduced a method to synthesize DNA nanostructures directly on magnetic beads, and the reaction performed in heavy liquid to maintain the beads in suspension. The solid phase synthesis protocol for folding DNA origami includes: scaffold, staple strands, magnetic beads and sodium polytungstate (SPT) in Tris-EDTA buffer. Magnetic beads were incubated at room temperature in Tris-EDTA buffer containing 250, 260, 270, 280, 290 and 300mM of SPT and imaged after 30 minutes, 1, 2 and 3 hours where we observed that SPT induces magnetic beads to remain in suspension for longer time when 250-270mM SPT was added to the mixture. An 18 helix bundle (18HB) DNA origami was tested with increasing concentrations of SPT (250-300mM) during folding. The sample was placed on a thermal cycler for a 16 hour folding program. With an external magnet, we captured the folded DNA origami and washed away the un-captured DNA origami as well as the excess of staple strands (unbound, U/B). Then we washed the sample three times, while only the first wash was run on the gel (W). Finally, the DNA origami bound on the beads was resuspended in Tris-EDTA buffer supplemented with 10mM MgCl2 and invasion strands. The sample was incubated under rotation and the DNA origami eluted from the beads (E). The unbound, wash and elution step samples from each folding reaction with 250-300mM SPT along with a reference structure, that was folded with the traditional method and purified with ultrafiltration columns, were run in an agarose gel. The reference structure was adjusted to a known concentration and the intensity of all bands were compared to it. By plotting the results in a bar plot from 4 individual experiments we observed that SPT concentrations between 250-280mM gave the highest folding yields.

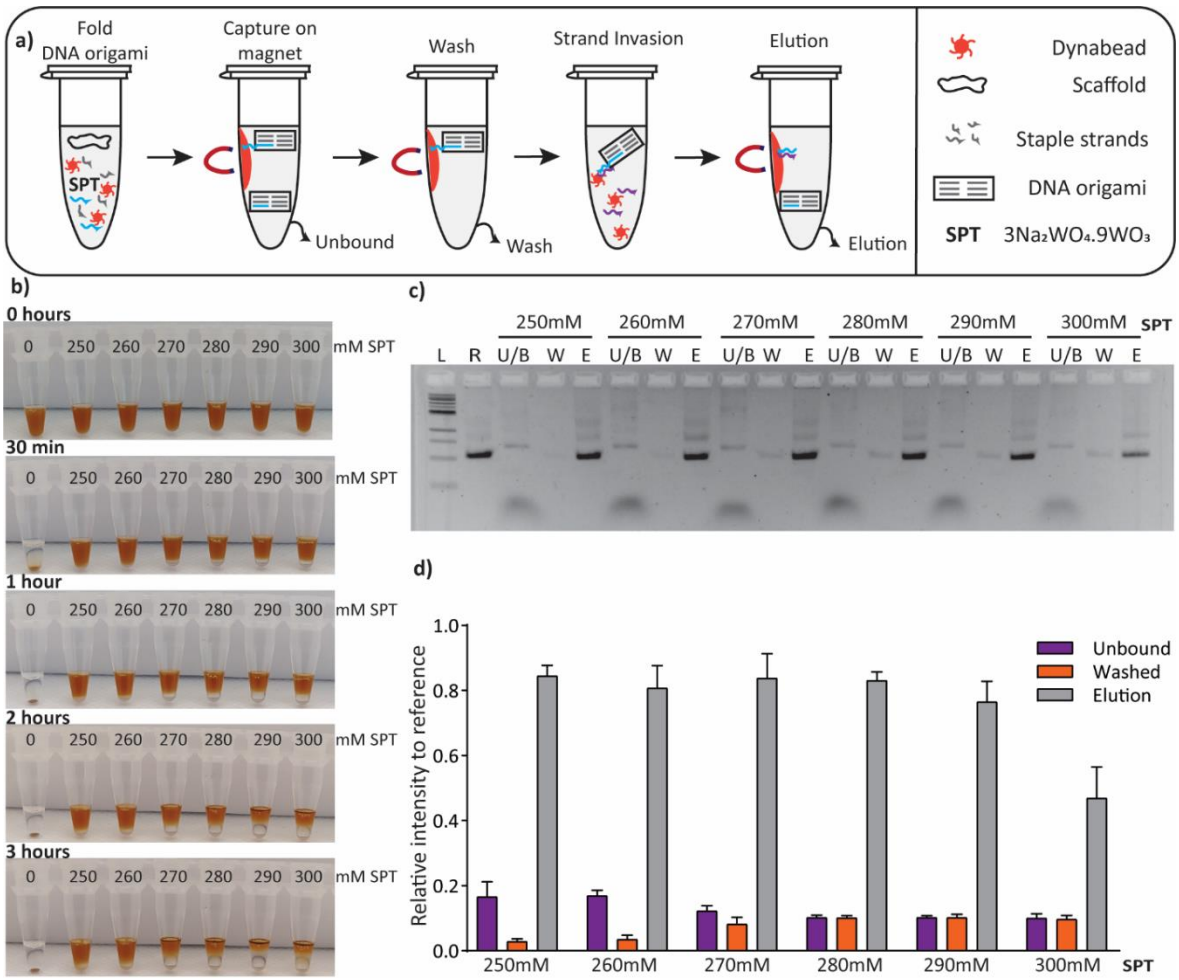

Figure 13. Folding of DNA origami on magnetic beads in suspension, using sodium polytungstate (SPT). a) DNA origami is folded by mixing magnetic beads, scaffold, staple strands and SPT in Tris-EDTA buffer. After folding, a magnet was used to capture magnetics beads with the origami, and the unbound origami and excess of staples are removed (Unbound). Additionally, washing buffer added to the beads, to assure that excess of material was removed (Wash). Magnetic beads with captured DNA origami re-suspend in elution buffer containing invasion strands. By placing a magnet, we capture only the beads, and the eluted DNA origami remains in solution (Elution). b) Images of magnetic beads re-suspended in 0mM and 250-300mM SPT on folding buffer at different time points up to 3 hours. c) Agarose gel of an 18 helix-bundle rod (18HB) DNA origami folded in 250, 260, 270, 280, 290 and 300mM SPT. Ladder 1kb (L), reference structures (R) and fractions of unbound (U/B), wash (W) and elution (E) steps ran on agarose gel. d) Intensity of each band measured and compared to a reference 18HB structure folded with a standard procedure. Standard deviations shown in bar plots from 4 individual experiments.

4.3.2 Optimization of the solid phase synthesis of DNA origami technique

To optimize the solid phase synthesis technique, we investigated the effect of $MgCl_2$, linker concentration, invader concentration, invader time and bead to DNA scaffold ratio on the reaction's folding yield (Figure 14). We first supplemented the reaction with different $MgCl_2$ concentrations, because typically close-packed DNA origami need $MgCl_2$ to keep the negatively charged phosphate backbone of the DNA helices to stay in close proximity. However, supplementing the folding reaction with $MgCl_2$ did not further improve the reaction yield. This could be explained by the fact that SPT solution contains sodium which is known to be able to replace $MgCl_2$ during folding reactions. Another factor tested was the concentration of the staples which links the DNA origami with the magnetic beads. Here we observed that the linker concentration should be in 10 times excess compared to scaffold concentration. To continue, we tested different ratio of ng scaffold per µl of beads during

folding where we conclude that 5.83ng scaffold /μl bead can result in up to 90% folding yield compared to a typical folding procedure. One more critical step for the solid phase synthesis of DNA origami is the invasion step that will facilitate the elution of the pure origami from the magnetic beads. Initially we tested increasing concentrations of invader strands, where we found that 25 times excess to scaffold concentration resulted in a sufficient DNA origami elution. The time that the invader needs for successful elution of DNA origami was found to be at least 1 hour.

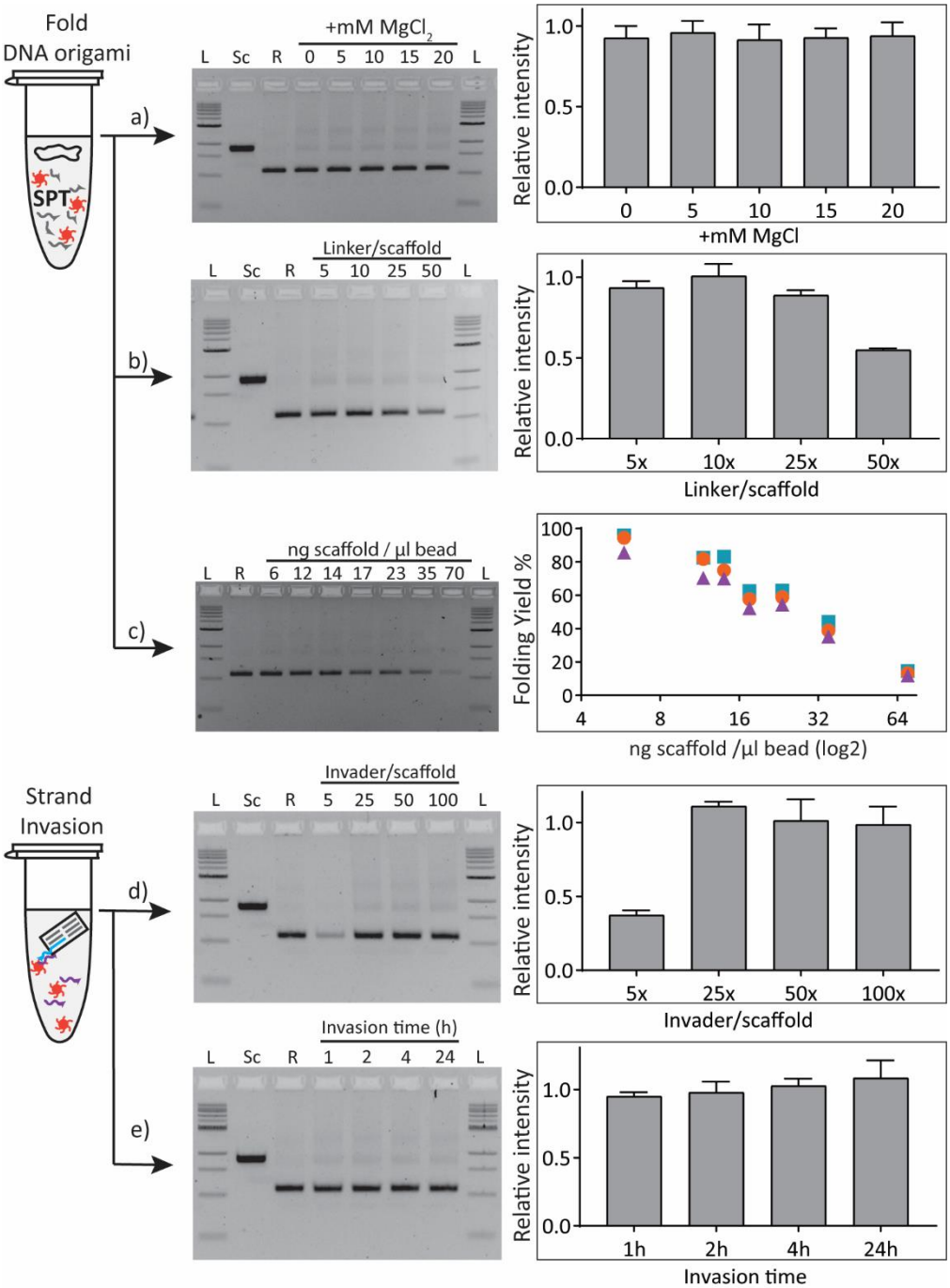

Figure 14. Optimization steps on solid phase synthesis of DNA origami. Five factors that affect the production efficiency tested on 18HB structure and fractions of elution samples ran in agarose gel. Intensity of the bands were measured and plotted according to their relative intensity compared to the reference structure. Samples ran in agarose gels are: 1kb ladder (L), scaffold (Sc), reference structure (R) and fractions of solid phase synthesis samples as described in each experiment: a) SPT in folding buffer supplemented with 5-20mM $MgCl_2$ during solid phase synthesis. b) 5-50 times excess of Linker to scaffold concentration tested during folding. c) 6-70 ng of

scaffold per µl of magnetic beads tested during folding and yield was calculated from the intensity of the bands compared to the intensity of reference product. Each symbol corresponds to individual experiment.

4.3.3 Folding different DNA nanostructures with the solid phase synthesis technique

The previous experiments were performed with the 18HB structure. To assure that our method gives good folding yields with different DNA origami we applied it on a 2D rectangle (R) structure and a hollow brick (HB) structure. All samples folded with 5.83ng scaffold /µl bead, scaffold, 5x excess of staples, 10x excess of linker to scaffold and 270mM SPT in Tris-EDTA buffer for 16hours at a thermal cycler. On the agarose gels we observe that a small amount of DNA origami remained unbound to the magnetic beads after folding and the excess of staples was successfully removed. The lanes of eluted samples migrated at the same speed with the reference structure and their corresponding samples showed identical geometries in TEM, indicating that the correct DNA shape folded with the solid phase synthesis technique (Figure15).

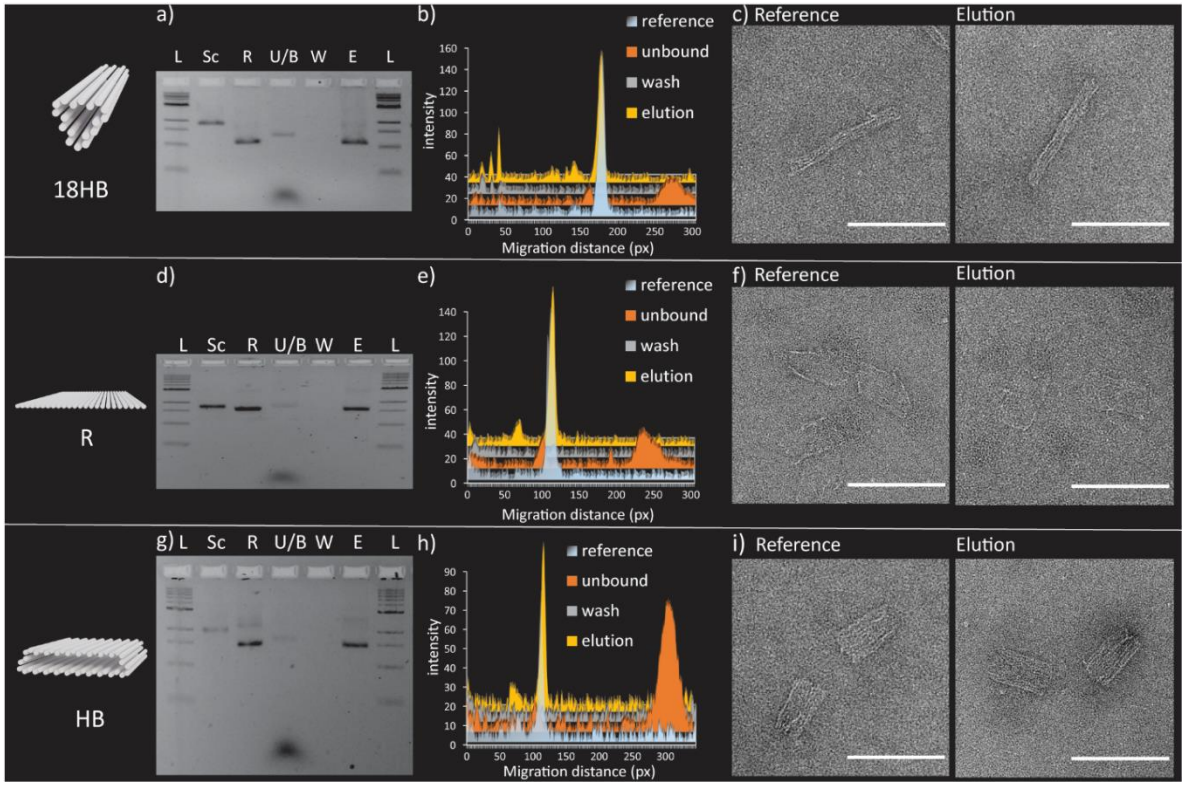

Figure 15. Different structures folded with the solid phase synthesis technique. Agarose gels for a) 18HB d) R and g) HB structures showing the migration of: 1kb ladder (L), scaffold (Sc), reference (R), unbound (U/B), wash (W) and elution (E) samples. b, e, h) Migration distance of each lane from agarose gels are shown on a plot. c, f, i) Sample TEM pictures of reference structures and structures from the solid phase synthesis for each case (scale bar 100nm).

4.4 PAPER IV

4.4.1 Optimization of hid-RT-PCR method

In paper IV we explored several factors that could establish an easy clinical protocol, for time and cost efficient detection of the virus SARS-CoV-2. The main technical procedure for diagnosing coronavirus disease 2019 in patient samples included: 1) RNA extraction of the

virus 2) reverse transcription of RNA to cDNA and 3) detection of the cDNA by real time PCR. In this study we aimed to develop a simplified method that could circumvent the RNA extraction step and replace the usage of transport media which, at the time of the study, were in short availability.

Our method development started by investigating the effect of transport media, used for swab sample collection, on real time PCR reaction. Synthetic SARS-CoV-2 RNA was spiked into three different transport media, and dilution series of the media were run on a single-reaction RT-PCR (Figure 16). The total reaction mixture is 20 μl and contained 10μl of sample and primer-probe for the nucleocapsid N1. From this experiment we concluded that inhibition of the reaction by the transport media was minimal when the amount was less the 25% in the RT-PCR reaction. We continued by testing the direct detection approach (excluding RNA extraction step) in clinical samples. We inactivated the samples either by adding MagNa Pure 96 external lysis buffer or by heating the samples at 65^{o}C for 30minutes. Here, we observed that samples inactivated with lysis buffer failed to give positive signal, while the same samples that were inactivated with heat, were correctly detected positive when compared to the traditional detection method. This heat inactivated direct RT-PCR (hid RT-PCR) procedure was further investigated. Another important factor of the RT-PCR protocol is the pair of primers with the probe against specific regions of the virus. For this reason, we tested primer-probe sets that target SARS-CoV-2 genes RNA-dependent RNA polymerase (RdRP), envelope (E), and nucleocapsid (N1). Clinical samples were heat inactivated (65^{o}C 30min), tested with different primer-probes and compared to detection with classical diagnostics. Here, we observed that N1 performs better than the other two genes, therefore we performed the following experiments with primer-probe for the N1 gene. Since we previously observed an inhibitory effect of the transport media to the RT-PCR reaction, we tested the input of heat inactivated clinical sample to the reaction mixture and found that loading 4 μl of sample into the 20 μl total reaction gives the optimal results. To further explore if the hid RT-PCR method is a reliable diagnostic tool for COVID-19 we tested it on 85 clinical diagnosed nasopharyngeal samples. We used 4μl sample input and primers for N1, RdRP with the hid-RT-PCR method and combined the results with clinical diagnostics after RNA extraction with primers for E and RdRP. Overall, most samples are in agreement between the two methods. Although, frozen heat inactivated samples appeared in higher Ct values compared to fresh eluted samples. This effect can be explained either by the damage caused from freeze and thaw cycles or by the smaller input volume of sample on hid-RT-PCR method (4μL) compared to the conventional RNA extraction method (10μl).

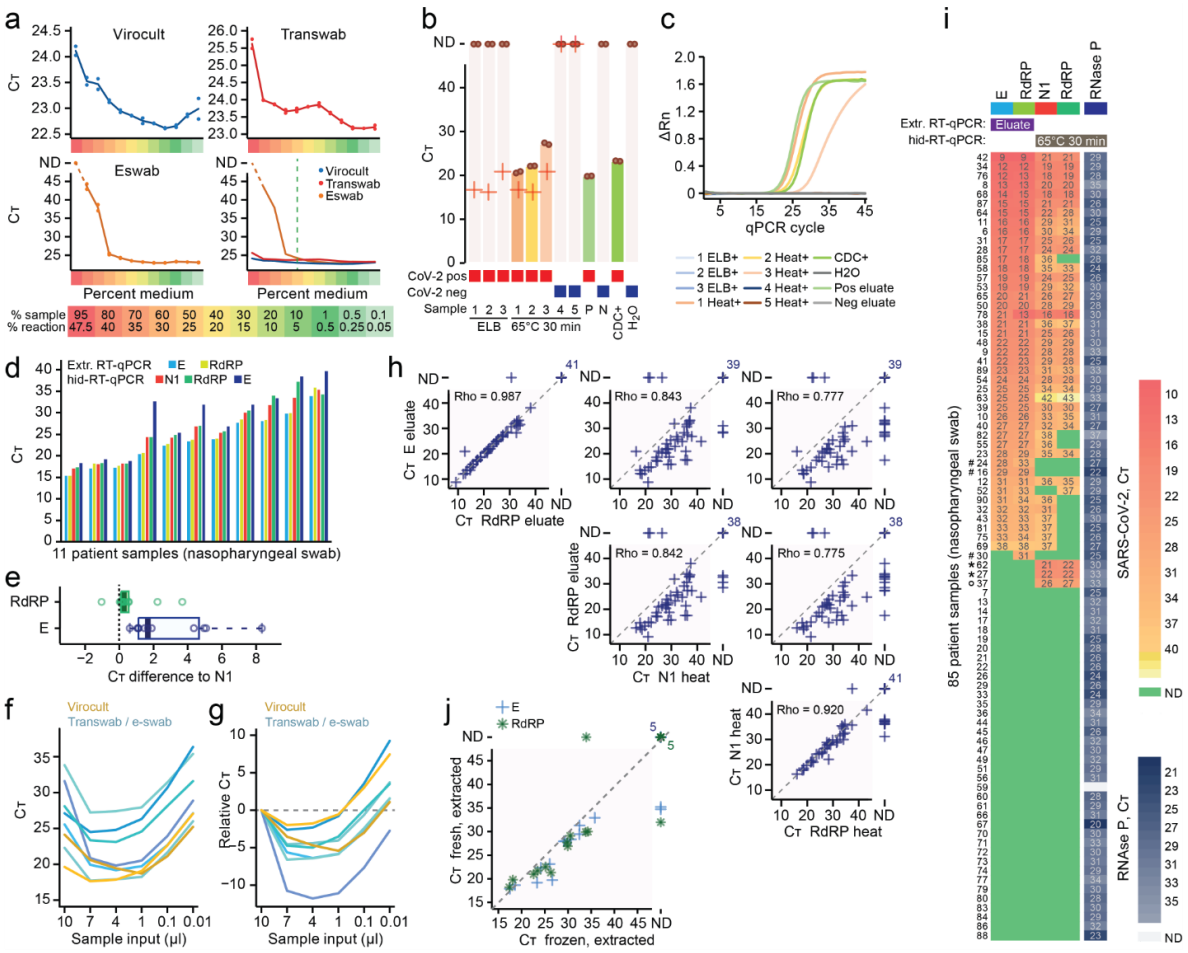

Figure 16. SARS-CoV-2 hid-RT-PCR on frozen nasopharyngeal swab samples. a) CT values from RT-qPCR performed on dilution series of transport medium (Virocult, Transwab, and Eswab) using 50,000 spiked copies of synthetic full-genome SARS-CoV-2 RNA and the N1 primer-probe set. Lines represent the mean of duplicates, shown individually as dots. ND: not detected. b) Bar plots of CT values from SARS-CoV-2 hid-RT-PCR on clinical nasopharyngeal swabs inactivated with MagNA Pure 96 External Lysis Buffer (ELB) or heat (65 °C 30 min). Dots indicate CT of hid-RT-PCR duplicates and crosses indicate CT values from diagnostics performed on fresh extracted RNA. Positive controls were extracted RNA from a positive sample (P) and a CDC positive control DNA plasmid (CDC+). Negative controls were extracted RNA from a negative sample (N) and water (H2O). ND: not detected. c) Amplification plots showing normalized reporter value (ΔRn, linear scale) as a function of qPCR cycle for the experiment and samples described in (b). (d) Bar plots of CT values of 11 positive nasopharyngeal swab samples using primer-probe sets targeting SARS-CoV-2 gene E, N, and RdRP. e) Boxplots of CT difference in same samples as in (d) comparing E and RdRP with the N1 primer-probe-set. Center lines denote the median, hinges denote the interquartile range (IQR) and whiskers denote outlier points at maximum 1.5 × IQR. f,g) Line charts of CT from individual clinical samples (colored lines) using variable amount of sample input. Shown as absolute CT (f) or CT relative to the 10µl input (g). h) Scatter plots of CT values from clinical diagnostics performed on extracted RNA (y-axis) and hid-RT-PCR (x-axis) of 85 nasopharyngeal swab samples, shown for different primer-probe set comparisons. Rho indicates Spearman correlation of positive samples. ND: not detected. i) Heatmap of CT values from diagnostics performed on 85 clinical samples using extracted RNA (E, RdRP) and hid-RT-PCR (N1, RdRP), ranked by E gene CT. Control for sample integrity by RT-PCR for RNase P in the same samples shown on the right. Two patients, marked with asterisk, were negative in extraction-based diagnostics but positive by hid-RT-PCR. The patients were later re-tested by extraction-based clinical diagnostics and confirmed to be SARS-CoV-2 positive. The patient marked with a ring was not re-tested. Three samples, marked with hash, were called COVID-19 positive by routine diagnostics but not by any primer-set in hid-RT-PCR. j) Scatter plot of CT values from 19 matched fresh (y-axis) and freeze-thawed (x-axis) extracted samples, using the E gene (cross) and RdRP (star) primer-probe sets. ND: not detected. hid-RT-PCR shown in this figure was performed on previously diagnosed frozen samples.

To identify a heat inactivation program that will improve our hid-RT-PCR method, we tested different incubation times (65°C 30 min; 95°C 5 min; 95°C 10 min; 95°C 15min; and 98°C 5min) to fresh nasopharyngeal sample stored in transport media. Our data showed Ct value

improvement, when we inactivated COVID19 samples at 95°C 5 min compared to 65°C 30 min. This is a positive improvement since better inactivation of the virus will be achieved at such high temperatures.

4.4.2 Generic buffers optimal for hid-RT-PCR method

Our previous data demonstrate that using general transport media (Virocult, Transwab, and Eswab) to collect clinical nasopharyngeal samples exerts limitations to the input volume of the samples in the hid-RT-PCR method. To improve our method, we needed to find collection buffers that would allow the maximum volume of sample into the real time PCR reaction. To explore this hypothesis, we spiked a fixed amount of active in vitro expanded SARS-CoV-2 in generic buffers easily accessible in a lab (Figure 17). We then performed heat inactivation at 95°C 5 min followed by real-time PCR using 4, 7, 10 and 13.5 µl input to a total of 20 µl reaction. Here, we identified many buffers that allow the maximum input to the pcr reaction mixture such as PVSA in nuclease-free water (50 µg/ml), TE, Tris buffer and nuclease-free water. When we stored the samples for 1, 4 and 7 days and tested them again, we observed that PVSA in water (pH 6.5) and 10 mM Tris buffer (pH 7) had unchangeable Ct values over the time. These buffers could be a cheap alternative solution to commercially available transport media that would permit a mass testing a samples.

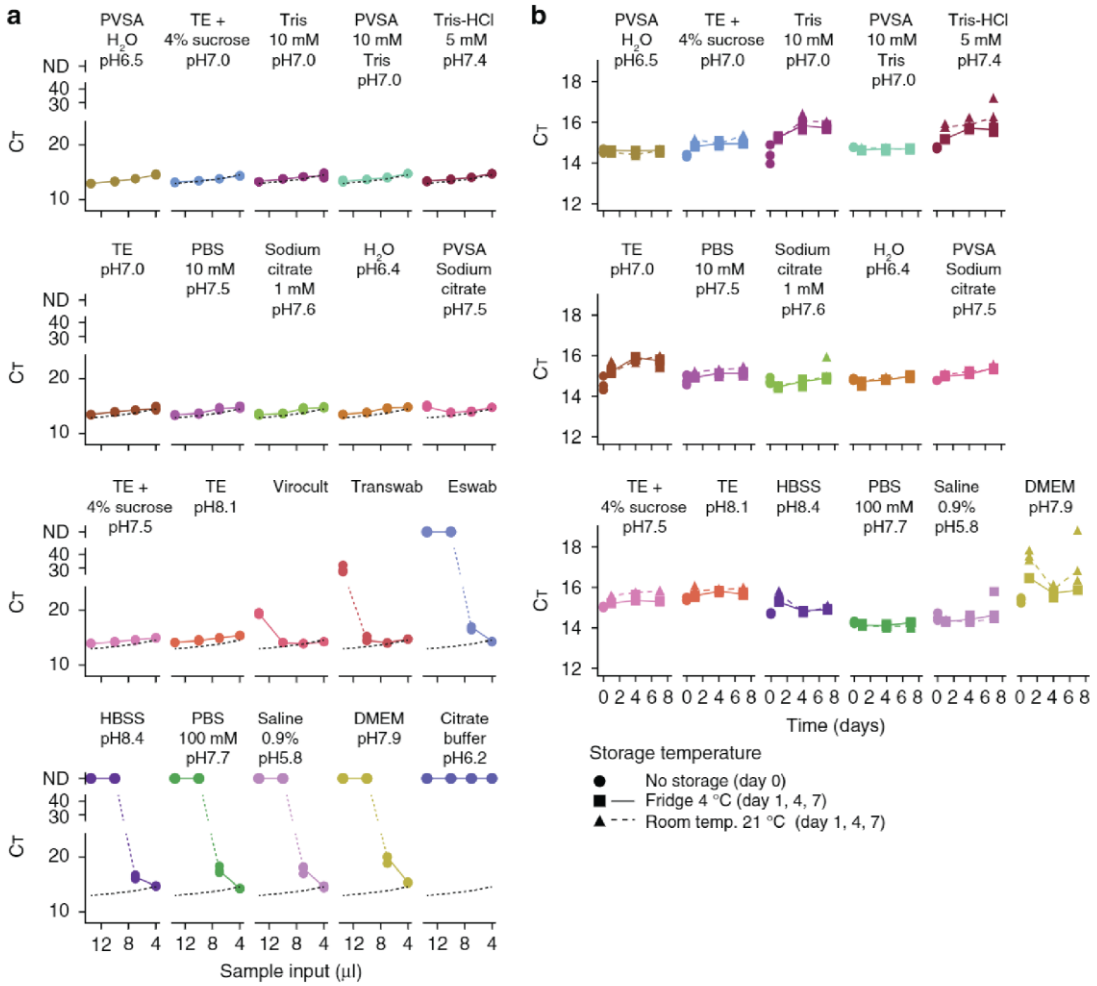

Figure 17 Identification of generic transport buffers optimal for SARS-CoV-2 hid-RT-PCR. A Line charts of CT values (y-axis) from hid-RT-PCR (N1 primer-probe pair) for different volume of input sample (13.5, 10, 7, or 4 µl to a20 µl reaction; x-axis), showing the inhibition profile of different transport buffers and media. The experiment was performed by adding equal amount of in vitro expanded SARS-CoV-2 to each buffer condition in experimental triplicates (dots). The dotted black lines indicate PVSA in H2O condition, included for comparison. The buffers are ordered according to minimal CT. b Line charts of CT values (y-axis) from hid-RT-PCR (N1 primer-probe pair, 4µl input to 20µl reactions) of in vitro expanded SARS-CoV-2 stored in different buffers for up to 7 days (x-axis) in fridge (4°C, square) or room temperature (21 °C, triangle) before subjecting the samples to heat inactivation (95°C 30 min) and hid-RT-PCR. The data are shown as individual replicates (points, n=3) and median (line)

5 CONCLUSIONS

The papers presented in this thesis showed that we were able to surpass previous limitations of existing molecular biology techniques by utilizing rationally designed probes from nucleic acids. DNA origami, due to its unique programmability characteristics, constitutes a precise tool for creating nanopatterns to enlighten our understanding on cell signaling and immunological responses.

In paper I, we used a patterned DNA origami to present antigens and measured the binding kinetics with their cognate antibodies. Specifically, we found that when antigens are separated at 3 to 17 nm distance the human IgG antibodies are binding bivalently with a distinct preference to 16nm distance. The binding profile changed when the affinity between antigens and antibodies was lower, but the peak binding affinity at 16nm remained. Moreover, differences in the antibody constant region showed to affect the binding strength with the antigen nanopatterns. IgM, which belongs to the first line of immune defense, showed a unique bivalent binding in a bigger range of antigen separation (3-29nm), when we studied a monomeric variant of IgM. Antibody producing cells initially express IgM and then switch to IgG a process known as differentiation and antibody class switch recombination. Our data suggest that more spatial tolerant antibodies are expressed at the first stage of immunological response and switch to the less spatial tolerant IgG, forcing the evolution towards antibodies that bind well in lower spatial tolerance.

In paper II, we investigated the effect of ligand cluster formation on Notch signaling pathway. We created patterns of Jag1 ligand displayed on a rod like DNA origami and by stimulating iPS derived neural progenitors, we found that bigger clusters of ligands induce higher activation of the Notch receptor. This clustering effect persisted when high concentrations of different clusters were tested, which excludes a correlation between high activation and nanopattern co-localization. We also demonstrated that the activation effect is happening in the absence of external forces which contradicts the main pulling of receptor hypothesis. On the other hand, when we increased the residence time of ligand receptor complex, we observed even higher activation levels of Notch receptor. All these results together led us to the conclusion that Notch receptor activation is affected by ligand cluster formation, which could result in prolonged binding of ligand receptor complexes in the absence of intercellular or external forces.

In paper III, we developed a new method to fold DNA origami directly on magnetic beads which serve as a fast purification tool directly after folding. We introduced the chemical compound sodium polytungstate (SPT) during folding in order to keep the beads in suspension and in parallel to provide the necessary positive charge for the DNA origami to form. We concluded that our method achieves up to 90% yield for several DNA origami shapes and extra modifications were successfully removed with the same solid support.

In paper IV, we explored procedures to circumvent RNA extraction step in protocols for detecting Covid19 in patient samples. We concluded that, by heat inactivating the samples, we

both inactivate the virus and we are able to detect with high accuracy the patients compare to standard diagnostic procedure. We showed the limitations of using commercial viral transport media with the hid-RT-PCR method and many alternative buffers were shown to preserve SARS-CoV2 storage over 7 days. Our data showed that our modified protocols for detecting Covid19 in patient samples could lead to scalable, rapid, and affordable diagnostics.

6 POINTS OF PERSPECTIVE

In paper I. we used patterns of antigens displayed on a DNA origami set up and found that antibodies bound with high affinity when antigens were separated by specific distances. Multivalent interactions between antigens and antibodies are known to be important for effector functions such as complement activation[73] and antibody-dependent cell-mediated cytotoxicity[74]. Since it is not known how specific patterns of multimerized antibodies affect antibody mediated functions, we could use the DNA origami technique, we have developed in this paper, to study the effect of different antibody patterns on downstream immunological processes.

In paper II. we suggested a different mode of activation for the Notch signaling pathway. We showed that the residence time of the receptor-ligand complex plays a crucial role in Notch receptor activation and that it is mediated primarily through the clustering of ligands, which affects this pathway by stabilizing their interaction to the receptors. Although, we do not know how this prolonged binding induces conformation changes of the receptor that results in the exposure of the NRR region. By using single molecule techniques and high resolution microscopy, changes in the distribution of individual ligand-receptor complexes upon treatment could be observed and correlated to receptor activation. Furthermore, we could create monomers and dimers of receptor-ligand complexes on a DNA origami structure, and conformational changes of the receptor upon ligand binding could be studied by using cryo-EM.

In paper III. we developed a method for folding and purifying DNA origami nanostructures. We found that sodium polytungstate (SPT) can create dense liquid solutions that keep magnetic beads in suspension for several hours. In the future, SPT could be used in other applications using magnetic beads, when stirring the reaction is prohibited. Additionally, our method could be applied on the emerging field of DNA origami superstructures[97,98] by using the magnetic beads for the step-wise assembly of complexes composed of several nanostructures.

In paper IV. we introduced a new protocol for detecting viral RNA in patient samples directly without RNA extraction. In our method we heat-inactivated the sample and then directly performed RT-PCR (hid-RT-PCR). This protocol could be used in the future for detecting different pathogens allowing large scale screening of the population in a fast and cheap way.

7 ACKNOWLEDGEMENTS

This thesis, is a cumulative result of working in the lab, during weekdays and weekends, developing collaborations, inside and outside Karolinska, and travelling to conferences to meet with scientists from multidisciplinary fields. I am grateful for all the people i met during this journey.

First of all, I would like to thank my supervisor, Björn Högberg, for giving me the opportunity to work on many ambitious and multidisciplinary projects, for triggering my excitement to explore new research paths and for his endless new ideas that opened up my scientific horizons. I would also like to thank my co-supervisor Ana Teixeira for welcoming me on the Notch project at the beginning of my PhD, and for sharing with me her scientific knowledge. Furthermore, I would like to thank Björn Reinius for the great collaboration we had, during such difficult times.

It was a great pleasure to work in the lab because of my amazing colleagues! I would like to thank Ferenc, for being always there for me as a friend and as a colleague. Thank you Yang for reminding me how it is to be excited with science and for being willing to work nights and weekends with me. Thank you Iris for accompanying me to the difficult path of Notch research. Thank you Marco and Igor for the nice moments we shared inside and outside of the lab. I would also like to thank Yunshi for always surprising us with amazing cakes. Thank you Boxuan, Alexander, Erik and Ieva for the great company and our scientific discussions. I would also like to thank Anurupa for bringing the lab together with food, candies and laughs.

Special thanks to the people that we shared our working environment in the past and are not members anymore. Thank you Mino for all the time we have spent together, the amazing Italian food and wine, and for the many more greek-italian days we will spend in the future! Thank you Erik for being my friend and for always inspiring me with your ideas inside and outside of science! I would also like to thank Alan for supervising me at the beginning of my PhD and the many early mornings, late nights and weekends we spent together in the lab! I would like to thank Joao and Esther for the moments we shared in the lab, outside the lab and for the ones we will share in the future. Thank you also Ian for our collaborations and your inspiring ideas and Giulio for all the knowledge you shared with me! Many thanks to my students Solrun and Till for working with me during their Masters.

Other people also in my working environment contributed with their own way to accomplish this goal. Thank you Chris and Natali for being my friends and for listening my lab related, or not, problems. Thanks Helene, Hannah, Magie, Hannes, Christina, Elena, Ekaterina, Joel and George for helping me to work on a nice environment.

I am very happy when I look back and I remember the moments I shared with my friends. Thank you Mino, Teresa and Cesare for being my family is Sweden! Anastasia, Alberto, Rania, Paschali, Ana-Maria, Konstantina, Maria, Gianni, Aki, Christine, Laurent, Daniela, Ben, Marta, Kyriaki and Viktoria for making my life happier! I am sorry if I forgot anyone who contributed to my happy moments in Sweden, your name should be here too _____☺

I want to thank my parents Andreas and Popi for raising me to be the person I am. My beloved brothers, Paris and Alexandros, for their endless love and support. Also my extended family Panikos, Athanasia, Christina, Yannis and Aliki for all the moments we spend together.

Finally, I would like to thank my husband Yannis, because he is making all my dreams possible. I am very lucky to have you in my life!

8 REFERENCES

1. Steve Minchin and Julia Lodge. Understanding biochemistry. structure and function of nucleic acids. Essays Biochem. 2019 Oct; 63(4): 433–456 (2019)

2. Krupovic M, Bamford DH. Double-stranded DNA viruses: 20 families and only five different architectural principles for virion assembly. *Curr Opin Virol*.;1(2):118-124 (2011)

3. V'kovski P, Kratzel A, Steiner S, Stalder H, Thiel V. Coronavirus biology and replication: implications for SARS-CoV-2. *Nat Rev Microbiol*.19(3):155-170. (2021)

4. Weber F, Wagner V, Rasmussen SB, Hartmann R, Paludan SR. Double-Stranded RNA Is Produced by Positive-Strand RNA Viruses and DNA Viruses but Not in Detectable Amounts by Negative-Strand RNA Viruses. *J Virol*.;80(10):5059-5064.(2006)

5. Felix D'Herelle. On an invisible microbe antagonistic toward dysenteric bacilli: brief note by Mr. F. D'Herelle, presented by Mr. Roux. *Res Microbiol*.;158(7):553-554. (2007)

6. Venkatesh S, Workman JL. Histone exchange, chromatin structure and the regulation of transcription. *Nat Rev Mol Cell Biol*.;16(3):178-189. (2015)

7. Crick F. Central dogma of molecular biology. *Nature*.;227(5258):561-563.(1970)

8. Statello L, Guo C-J, Chen L-L, Huarte M. Gene regulation by long non-coding RNAs and its biological functions. *Nat Rev Mol Cell Biol*. 22, 96–118 (2021)

9. Seeman NC. Nucleic acid junctions and lattices. *J Theor Biol*.;99(2):237-247.(1982)

10. Chen J, Seeman NC. *Synthesis from DNA of a Molecule with the Connectivity of a Cube*. Vol 50.; (1987)

11. Winfree E, Liu F, Wenzler LA, Seeman NC. Design and self-assembly of two-dimensional DNA crystals. *Nature*.;394(6693):539-544.(1998)

12. Jianping Zheng, Jens J. Birktoft, Yi Chen, Tong Wang, Ruojie Sha, Pamela E. Constantinou, Stephan L. Ginell, Chengde Mao & Nadrian C. Seeman. From molecular to macroscopic via the rational design of a self-assembled 3D DNA crystal. *Nature*.;461(7260):74-77 (2009)

13. Shih WM, Quispe JD, Joyce GF. A 1.7-kilobase single-stranded DNA that folds into a nanoscale octahedron. *Nature*.;427(6975):618-621.(2004)

14. Rothemund PWK. Folding DNA to create nanoscale shapes and patterns. *Nature*.;440(7082):297-302 (2006)

15. Douglas SM, Dietz H, Liedl T, Högberg B, Graf F, Shih WM. Self-assembly of DNA into nanoscale three-dimensional shapes. *Nature*.;459(7245):414-418.(2009)

16. Douglas SM, Marblestone AH, Teerapittayanon S, Vazquez A, Church GM, Shih WM. Rapid prototyping of 3D DNA-origami shapes with caDNAno. *Nucleic Acids Res*.;37(15):5001-5006 (2009)

17. Ke Y, Douglas SM, Liu M, et al. Multilayer DNA origami packed on a square lattice. *J Am Chem Soc*.;131(43):15903-15908 (2009)

18. Dietz H, Douglas SM, Shih WM. Folding DNA into twisted and curved nanoscale shapes. *Science (80-).*;325(5941):725-730 (2009)

19. Han D, Pal S, Nangreave J, Deng Z, Liu Y, Yan H. DNA origami with complex curvatures in three-dimensional space. *Science (80-).*;332(6027):342-346 (2011)

20. Erik Benson, Abdulmelik Mohammed, Johan Gardell, Sergej Masich, Eugen Czeizler, Pekka Orponen & Björn Högberg. DNA rendering of polyhedral meshes at the nanoscale. 523, 441–444 (2015)

21. Fei Zhang, Shuoxing Jiang, Siyu Wu, Yulin Li, Chengde Mao, Yan Liu & Hao Yan. Complex wireframe DNA origami nanostructures with multi-arm junction vertices. Nature Nanotech 10, 779–784 (2015)

22. Benson E, Mohammed A, Rayneau-kirkhope D, Gådin A, Orponen P. Effects of Design Choices on the Sti ff ness of Wireframe DNA Origami Structures. ACS Nano 12, 9, 9291–9299 (2018)

23. Nanda JS, Lorsch JR. *Labeling a Protein with Fluorophores Using NHS Ester Derivitization*. Methods in Enzymology Vol 536. 1st ed. Elsevier Inc.; (2014)

24. Cole NB. Site-specific protein labeling with SNAP-tags. *Curr Protoc Protein Sci. Sep 24; 73: 30.1.1–30.1.16. (2013)*

25. Gurard-levin ZA, Kilian KA, Kim J, Ba K. HaloTag: A Novel Protein Labeling Technology for Cell Imaging and Protein Analysis. *ACS Chem Biol*.;60(9):45-58 (2010)

26. Arnaud Gautier 1, Alexandre Juillerat, Christian Heinis, Ivan Reis Corrêa Jr, Maik Kindermann, Florent Beaufils, Kai Johnsson. An Engineered Protein Tag for Multiprotein Labeling in Living Cells. *Chem Biol*.;15(2):128-136 (2008)

27. Daniel Hatlem , Thomas Trunk , Dirk Linke , Jack C Leo. Catching a SPY Using the SpyCatcher SpyTag and Related Systems for Labeling and Localizing Bacterial Protein. Int J Mol Sci Apr 30;20(9):2129 (2019)

28. Fan C, Ip K, Söll D. Expanding the genetic code of Escherichia coli with phosphotyrosine. *FEBS Lett*.;292(April):3040-3047 (2016)

29. Jennifer Z. Yao, Chayasith Uttamapinant, Andrei Poloukhtine, Jeremy M. Baskin, Julian A. Codelli, Ellen M. Sletten, Carolyn R. Bertozzi, Vladimir V. Popik, and Alice Y. Ting. Fluorophore Targeting to Cellular Proteins via Enzyme-Mediated Azide Ligation and Strain-Promoted Cycloaddition. J. Am. Chem. Soc. 134, 8, 3720–3728 (2012)

30. Ton-That H, Liu G, Mazmanian SK, Faull KF, Schneewind O. Purification and characterization of sortase, the transpeptidase that cleaves surface proteins of Staphylococcus aureus at the LPXTG motif. *Proc Natl Acad Sci U S A*.;96(22):12424-12429. (1999)

31. Chad R. Simmons, Fei Zhang, Tara MacCulloch, Noureddine Fahmi, Nicholas Stephanopoulos, Yan Liu, Nadrian C. Seeman, and Hao Yan. Tuning the Cavity Size and Chirality of Self-Assembling 3D DNA Crystals. . Am. Chem. Soc., 139, 32, 11254–11260 (2017)

32. Chad R. Simmons, Fei Zhang, Jens J. Birktoft, Xiaodong Qi, Dongran Han, Yan Liu, Ruojie Sha, Hatem O. Abdallah, Carina Hernandez, Yoel P. Ohayon, Nadrian C. Seeman, and Hao Yan. Construction and Structure Determination of a Three-

Dimensional. J. Am. Chem. Soc., 138, 31, 10047–10054 (2016)

33. Stahl E, Praetorius F, Mann O, Hopfner K, Dietz H. Impact of Heterogeneity and Lattice Bond Strength on DNA Triangle Crystal Growth. ACS Nano, 10, 10, 9156–9164 (2016)

34. Bai X-C, Martin TG, Scheres SHW, Dietz H. Cryo-EM structure of a 3D DNA-origami PNAS November 19, 109 (49) 20012-20017 (2012)

35. Thomas G. Martin, Tanmay A. M. Bharat, Andreas C. Joerger, Xiao-chen Bai, Florian Praetorius, Alan R. Fersht, Hendrik Dietz scheres and Sjors H. W. Scheres. Design of a molecular support for cryo-EM structure determination. PNAS 113 (47) E7456-E7463 (2016)

36. Tural Aksel, Zanlin Yu, Yifan Cheng & Shawn M. Douglas. Molecular goniometers for single-particle cryo-EM of DNA-binding proteins. Nat Biotechnol 39, 378–386 (2021)

37. Emma Silvester, Benjamin Vollmer, Vojtěch Pražák, Daven Vasishtan, Emily A.Machala, Catheryne Whittle, Susan Black, Jonathan Bath, Andrew J.Turberfield, Kay Grünewald, Lindsay A. Baker. DNA origami signposts for identifying proteins on cell membranes by electron cryotomography. *Cell*.;184(4):1110-1121.e16. (2021)

38. Bath J, Turberfield AJ. DNA nanomachines. *Nat Nanotechnol*.;2(5):275-284. (2007)

39. Kuzuya A, Ohya Y. Nanomechanical molecular devices made of DNA origami. *Acc Chem Res*.;47(6):1742-1749. (2014)

40. Peng Yin 1, Hao Yan, Xiaoju G Daniell, Andrew J Turberfield, John H Reif. A Unidirectional DNA Walker That Moves Autonomously along a Track. *Angew Chem Int Ed*.;43:4906-4911 (2004)

41. Shin JS, Pierce NA. A synthetic DNA walker for molecular transport. *J Am Chem Soc*.;126(35):10834-10835 (2004)

42. Mingxu You,Dr. Yan Chen,Prof. Dr. Xiaobing Zhang,Dr. Haipeng Liu,Dr. Ruowen Wang,Dr. Kelong Wang,Dr. Kathryn R. Williams,Prof. Dr. Weihong Tan. An autonomous and controllable light-driven DNA walking device. *Angew Chemie - Int Ed*.;51(10):2457-2460. (2012)

43. Yurke B, Turberfield AJ, Mills AP, Simmel FC, Neumann JL. A DNA-fuelled molecular machine made of DNA. *Nature*.;406(6796). (2000)

44. Gerling T, Wagenbauer KF, Neuner AM, Dietz H. Dynamic DNA devices and assemblies formed by shape-complementary, non-base pairing 3D components. *Science (80-).*;347(6229):1446-1452.(2015)

45. Erik Benson, Rafael Carrascosa Marzo, Jonathan Bath AJT. A DNA molecular printer capable of programmable positioning and patterning in two. Science;7(February):1-31 (2021)

46. Funke JJ, Dietz H. Placing molecules with Bohr radius resolution using DNA origami. *Nat Nanotechnol*.; 11, pages 47–52.(2015)

47. Funke JJ, Ketterer P, Lieleg C, Schunter S, Korber P, Dietz Hendrik. *Uncovering the Forces between Nucleosomes Using DNA Origami*. Sci Adv Nov 23;2(11):e1600974 (2016)

48. Yong-Xing Zhao, Alan Shaw, Xianghui Zeng, Erik Benson, Andreas M. Nyström, and

Björn Högberg. DNA Origami Delivery System for Cancer Therapy with Tunable Release Properties. ACS Nano 6, 10, 8684–8691(2012)

49. Qiao Jiang, Chen Song, Jeanette Nangreave, Xiaowei Liu, Lin Lin, Dengli Qiu, Zhen-Gang Wang, Guozhang Zou, Xingjie Liang, Hao Yan, and Baoquan Ding. DNA origami as a carrier for circumvention of drug resistance. *J Am Chem Soc*.;134(32):13396-13403.(2012)

50. Patrick D Halley, Christopher R Lucas, Emily M McWilliams, Matthew J Webber, Randy A Patton, Comert Kural, David M Lucas, John C Byrd, Carlos E Castro. Daunorubicin-Loaded DNA Origami Nanostructures Circumvent Drug-Resistance Mechanisms in a Leukemia Model. *Small*.;12(3):308-320.(2016)

51. Qian Zhang, Qiao Jiang, Na Li, Luru Dai, Qing Liu, Linlin Song, Jinye Wang, Yaqian Li, Jie Tian, Baoquan Ding, and Yang Du. DNA origami as an in vivo drug delivery vehicle for cancer therapy. *ACS Nano*.;8(7):6633-6643.(2014)

52. Douglas SM, Bachelet I. A Logic-Gated Nanorobot for Targeted Transport of Molecular Payloads. Science Vol 335, Issue 6070 pp. 831-834 (2012)

53. Suping Li, Qiao Jiang, Shaoli Liu, Yinlong Zhang, Yanhua Tian, Chen Song, Jing Wang, Yiguo Zou, Gregory J Anderson, Jing-Yan Han, Yung Chang, Yan Liu, Chen Zhang, Liang Chen, Guangbiao Zhou, Guangjun Nie, Hao Yan, Baoquan Ding & Yuliang Zhao. A DNA nanorobot functions as a cancer therapeutic in response to a molecular trigger in vivo. *Nat Biotechnol 36, 258–264 (2018)*

54. Perrault SD, Shih WM. Virus-inspired membrane encapsulation of DNA nanostructures to achieve in vivo stability. *ACS Nano, 8, 5, 5132–5140(2014)*

55. Nandhini Ponnuswamy, Maartje M. C. Bastings, Bhavik Nathwani, Ju Hee Ryu, Leo Y. T. Chou, Mathias Vinther, Weiwei Aileen Li, Frances M. Anastassacos, David J. Mooney & William M. Shih. Oligolysine-based coating protects DNA nanostructures from low-salt denaturation and nuclease degradation. *Nat Commun 8, 15654 (2017)*

56. Jinglin Fu, Minghui Liu, Yan Liu, Neal W. Woodbury, and Hao Yan. Interenzyme Substrate Diffusion for an Enzyme Cascade Organized on Spatially Addressable DNA Nanostructures. J. Am. Chem. Soc. 134, 12, 5516–5519 (2012)

57. Jinglin Fu, Yuhe Renee Yang, Soma Dhakal, Zhao Zhao, Minghui Liu, Ting Zhang, Nils G Walter & Hao Yan. Assembly of multienzyme complexes on DNA nanostructures. *Nat Protoc 11, 2243–2273 (2016)*

58. Guoliang Ke, Minghui Liu, Shuoxing Jiang, Xiaodong Qi, Yuhe Renee Yang, Shaun Wootten, Fei Zhang, Zhi Zhu, Yan Liu, Chaoyong James Yang, Hao Y. Directional Regulation of Enzyme Pathways through the Control of Substrate Channeling on a DNA Origami Scaffold. Angew Chem Int Ed Engl Jun 20;55(26):7483-6 (2016)

59. Zhao Zhao, Jinglin Fu, Soma Dhakal, Alexander Johnson-Buck, Minghui Liu, Ting Zhang, Neal W. Woodbury, Yan Liu, Nils G. Walter & Hao Yan. Nanocaged enzymes with enhanced catalytic activity and increased stability against protease digestion. *Nat Commun 7, 10619 (2016)*

60. Sharonov A, Hochstrasser RM. Wide-field subdiffraction imaging by accumulated binding of diffusing probes. PNAS 103 (50) 18911-18916 (2016)

61. Pasquale EB. Eph receptors and ephrins in cancer: Bidirectional signalling and beyond. *Nat Rev Cancer*.;10(3):165-180. (2010)

62. Alan Shaw, Vanessa Lundin, Ekaterina Petrova, Ferenc Fördős, Erik Benson, Abdullah Al-Amin, Anna Herland, Andries Blokzijl, Björn Högberg & Ana I Teixeira. Spatial control of membrane receptor function using ligand nanocalipers. *Nat Methods*.;11(8):841-846 (2014)

63. Toon Verheyen, Trixy Fang, Dominik Lindenhofer, Yang Wang, Karen Akopyan, Arne Lindqvist, Björn Högberg, Ana I Teixeira. Spatial organization-dependent EphA2 transcriptional responses revealed by ligand nanocalipers. *Nucleic Acids Res*.;48(10):5777-5787. (2020)

64. Alessandro Angelin,Simone Weigel,Ruben Garrecht,Dr. Rebecca Meyer,Jens Bauer,Ravi Kapoor Kumar,Dr. Michael Hirtz,Prof. Dr. Christof M. Niemeyer. Multiscale Origami Structures as Interface for Cells. *Angew Chemie - Int Ed*.;54(52). (2015)

65. Patel K, Perez-garrido S, Marshall JF, Palma M. DNA Origami Nanoarrays for Multivalent Investigations of Cancer Cell Spreading with Nanoscale Spatial Resolution and Single- Molecule Control. ACS Nano , 13, 1, 728–736 (2019)

66. Kurisinkal EE, Caroprese V, Koga MM, Morzy D, Bastings MMC. Selective Integrin α5β1 Targeting through Spatially Constrained Multivalent DNA-Based Nanoparticles. *Molecules*.;27(15):4968. (2022)

67. Liqiang Pan, Tian-Min Fu, Wenbin Zhao, Linlin Zhao, Wen Chen, Chixiao Qiu, Wenhui Liu, Zhijun Liu, Alessandro Piai, Qingshan Fu, Shuqing Chen, Hao Wu, James J Chou. Higher-Order Clustering of the Transmembrane Anchor of DR5 Drives Signaling. *Cell*.;176(6):1477-1489.e14.(2019)

68. Wang Y, Baars I, Fördös F, Högberg B. Clustering of Death Receptor for Apoptosis Using Nanoscale Patterns of Peptides. *ACS Nano*.;15(6). (2021)

69. Ricarda M. L. Berger,Johann M. Weck,Simon M. Kempe,Oliver Hill,Tim Liedl,Joachim O. Rädler,Cornelia Monzel,Amelie Heuer-Jungemann. Nanoscale FasL Organization on DNA Origami to Decipher Apoptosis Signal Activation in Cells. *Small*.;17(26). (2021)

70. Jr, Charles A. Janeway, Paul Travers, Mark Walport MJS. *Immunobiology:The Immune System in Helth and Disease*. Garland Science; 2001.5th edition

71. Xing Zhang, Lei Zhang, Huimin Tong, Bo Peng, Matthew J. Rames, Shengli Zhang & Gang Ren. 3D Structural Fluctuation of IgG1 Antibody Revealed by Individual Particle Electron Tomography. *Sci Rep*. 2015;5(1):9803.(2015)

72. Erica Ollmann Saphire, Paul W. H. I. Parren, Ralph Pantophlet, Michael B. Zwick, Garrett M. Morris, Pauline M. Rudd, Raymond A. Dwek, Robyn L. Stanfield,1 Dennis R. Burton, Ian A. Wilson. Crystal Structure of a Neutralizing Human IgG Against HIV-1: A Template for Vaccine Design. *Science Aug 10;293(5532):1155-9 (2001)*

73. Christoph A Diebolder 1, Frank J Beurskens, Rob N de Jong, Roman I Koning, Kristin Strumane, Margaret A Lindorfer, Marleen Voorhorst, Deniz Ugurlar, Sara Rosati, Albert J R Heck, Jan G J van de Winkel, Ian A Wilson, Abraham J Koster, Ronald P Taylor, Erica Ollmann Saphire, Dennis R Burton, Janine Schuurman, Piet Gros, Paul W H I Parren. Complement Is Activated by IgG Hexamers Assembled at the Cell Surface.

Science. Mar 14;343(6176):1260-3 (2014)

74. Sondermann P, Huber R, Oosthuizen V, Jacob U. The 3.2-A crystal structure of the human IgG1 Fc fragment-Fc gammaRIII complex. Nature Jul 20;406(6793):267-73.(2000)

75. Shuo-Wang Qiao 1, Kanna Kobayashi, Finn-Eirik Johansen, Ludvig M Sollid, Jan Terje Andersen, Edgar Milford, Derry C Roopenian, Wayne I Lencer, Richard S Blumberg. Dependence of antibody-mediated presentation of antigen on FcRn. *Proc Natl Acad Sci*.;105(27):9337-9342. (2008)

76. Puffer EB, Pontrello JK, Hollenbeck JJ, Kink JA, Kiessling LL. Activating B cells signalling with defined multivalent ligands. *ACS Chem Biol*.;2(4):252-262. (2007)

77. Minguet S, Dopfer EP, Schamel WWA. Low-valency, but not monovalent, antigens trigger the B-cell antigen receptor (BCR). *Int Immunol*.;22(3):205-212. (2010)

78. Veneziano R, Moyer TJ, Stone MB, et al. Role of nanoscale antigen organization on B-cell activation probed using DNA origami. *Nat Nanotechnol*.;15(8):716-723. (2020)

79. Teixeira AI, Fang T, Alvelid J, Spratt J, Ambrosetti E, Testa I. Spatial regulation of t-cell signaling by programmed death-ligand 1 on wireframe DNA origami flat sheets. *ACS Nano*.;15(2). (2021)

80. Alice Comberlato, Marianna M. Koga, Simone Nüssing, Ian A. Parish, and Maartje M. C. Bastings. Spatially Controlled Activation of Toll like Receptor 9 with DNA Based Nanomaterials. Nano Lett., 22, 6, 2506–2513 (2022)

81. Kern N, Dong R, Douglas SM, Vale RD, Morrissey MA. Tight nanoscale clustering of fcγ receptors using dna origami promotes phagocytosis. *Elife*.;10:1-29. (2021)

82. Oren Shaya, Udi Binshtok, Micha Hersch, Dmitri Rivkin, Sheila Weinreb, Liat Amir-Zilberstein, Bassma Khamaisi, Olya Oppenheim, Ravi A Desai, Richard J Goodyear, Guy P Richardson, Christopher S Chen, David Sprinzak. Cell-Cell Contact Area Affects Notch Signaling and Notch-Dependent Patterning. *Dev Cell*.;40(5):505-511.e6. (2017)

83. Sanchez-Irizarry C, Carpenter AC, Weng AP, Pear WS, Aster JC, Blacklow SC. Notch Subunit Heterodimerization and Prevention of Ligand-Independent Proteolytic Activation Depend, Respectively, on a Novel Domain and the LNR Repeats. *Mol Cell Biol*.;24(21):9265-9273 (2004)

84. Chandramouli R Chillakuri 1, Devon Sheppard, Ma Xenia G Ilagan, Laurie R Holt, Felicity Abbott, Shaoyan Liang, Raphael Kopan, Penny A Handford, Susan M Lea. Structural Analysis Uncovers Lipid-Binding Properties of Notch Ligands. *Cell Rep*.;5(4):861-867.(2013)

85. Luca VC, Jude KM, Pierce NW, Nachury M V., Fischer S, Garcia KC. Structural basis for Notch1 engagement of Delta-like 4. *Science (80-)*.;347(6224):847-853. (2015)

86. Kakuda S, Haltiwanger RS, Kakuda S, Haltiwanger RS. Short Article Deciphering the Fringe-Mediated Notch Code : Identification of Activating and Inhibiting Sites Allowing Discrimination between Ligands Short Article Deciphering the Fringe-Mediated Notch Code : Identification of Activating and Inhibiting Sit. *Dev Cell*.;40(2):193-201. (2017)

87. Rios AC, Serralbo O, Salgado D, Marcelle C. Neural crest regulates myogenesis through

the transient activation of NOTCH. Nature 473, 532–535 (2011)

88. Cappellari O, Benedetti S, Innocenzi A, et al. Dll4 and PDGF-BB Convert Committed Skeletal Myoblasts to Pericytes without Erasing Their Myogenic Memory. *Dev Cell*.;24(6):586-599. (2013)

89. Parks AL, Klueg KM, Stout JR, Muskavitch MAT. Ligand endocytosis drives receptor dissociation and activation in the Notch pathway. *Development*.;127(7):1373-1385. (2000)

90. G Chapman, J A Major, K Iyer, A C James, S E Pursglove, J L M Moreau, S L Dunwoodie. Notch1 endocytosis is induced by ligand and is required for signal transduction. Biochim Biophys Acta Jan;1863(1):166-77.(2016)

91. Langridge PD, Struhl G. Epsin-Dependent Ligand Endocytosis Activates Notch by Force. *Cell*.;171:1383-1396. (2017)

92. Wang X, Ha T. Defining single molecular forces required to activate integrin and Notch signaling. *Science (80-).*;340(6135):991-994. (2013)

93. Gordon WR, Zimmerman B, He L, Perrimon N, Loparo JJ, Blacklow SC. Mechanical Allostery: Evidence for a Force Requirement in the Proteolytic Activation of Notch. *Dev Cell*.;33:729-736. (2015)

94. Vincent C Luca, Byoung Choul Kim, Chenghao Ge, Shinako Kakuda, Di Wu, Mehdi Roein-Peikar, Robert S Haltiwanger, Cheng Zhu, Taekjip Ha, K Christopher Garcia. Notch-Jagged complex structure implicates a catch bond in tuning ligand sensitivity. Science Mar 24;355(6331):1320-1324 (2017)

95. Nandagopal N, Santat LA, LeBon L, Sprinzak D, Bronner ME, Elowitz MB. Dynamic Ligand Discrimination in the Notch Signaling Pathway. *Cell*.;172(4):869-880.e19. (2018)

96. Douglas SM, Marblestone AH, Teerapittayanon S, Vazquez A, Church GM, Shih WM. Rapid prototyping of 3D DNA-origami shapes with caDNAno. *Nucleic Acids Res*.;37(15):5001-5006. (2009)

97. Yao G, Zhang F, Wang F, et al. Meta-DNA structures. *Nat. Chem. 12, 1067–1075 (2020)*

98. Minev D, Wintersinger CM, Ershova A, Shih WM. Robust nucleation control via crisscross polymerization of highly coordinated DNA slats. *Nat Commun 12, 1741 (2021).*